Inorg. Chem. **2004**, *43*, 7014–7029

Solid-State Coordination Chemistry of the Oxomolybdate–Organodiphosphonate/Nickel–Organoimine System: Structural Influences of the Secondary Metal Coordination Cation and Diphosphonate Tether Lengths

Eric Burkholder,[†] Vladimir Golub,[‡] Charles J. O'Connor,[‡] and Jon Zubieta*[,†]

Department of Chemistry, Syracuse University, Syracuse, New York 13244, and Department of Chemistry, University of New Orleans, New Orleans, Louisiana 70148

Received June 18, 2004

The hydrothermal reactions of a molybdate source, a nickel(II) salt, tetra-2-pyridylpyrazine (tpyprz), and organodiphosphonic acids $H_2O_3P(CH_2)_nPO_3H_2$ (n = 1–5) of varying tether lengths yielded a series of organic–inorganic hybrid materials of the nickel–molybdophosphonate family. A persistent characteristic of the structural chemistry is the presence of the $\{Mo_5O_{15}(O_3PR)_2\}^{4-}$ cluster as a molecular building block, as noted for the one-dimensional materials $[\{Ni_2(tpyprz)_2\}Mo_5O_{15}\{O_3P(CH_2)_4PO_3\}]\cdot 6.65H_2O$ (**6**·6.65H_2O) and $[\{Ni_2(tpyprz)_2\}Mo_5O_{15}\{O_3P(CH_2)_5PO_3\}]\cdot 3.75H_2O$ (**8**·3.75H_2O), the two-dimensional phases $[\{Ni_4(tpyprz)_3\}\{Mo_5O_{15}(O_3PCH_2CH_2PO_3)\}_2]\cdot 23H_2O$ (**3**·23H_2O) and $[\{Ni_3(tpyprz)_2(H_2O)_2\}(Mo_5O_{15})(Mo_2O_4F_2)\{O_3P(CH_2)_3PO_3\}_2]\cdot 8H_2O$ (**5**·8H_2O), and the three-dimensional structures $[\{Ni_2(tpyprz)(H_2O)_3\}Mo_5O_{15}\{O_3P(CH_2)_3PO_3)\}]\cdot H_2O$ (**4**·H_2O) and $[\{Ni_2(tpyprz)(H_2O)_2\}Mo_5O_{15}\{O_3P(CH_2)_4PO_3\}]\cdot 2.25H_2O$ (**7**·2.25H_2O). In the case of methylenediphosphonic acid, the inability of this ligand to tether adjacent pentanuclear clusters precludes the formation of the common molybdophosphonate building block, manifesting in contrast a second structural motif, the trinuclear $\{(Mo_3O_8)_x(O_3PCH_2PO_3)_y\}$ subunit of $[\{Ni(tpyprz)(H_2O)_2\}(Mo_3O_8)_2(O_3PCH_2PO_3)_2]$ (**1**) which had been previously observed in the corresponding methylenediphosphonate phases of the copper–molybdophosphonate family. Methylenediphosphonic acid also provides a second phase, $[Ni_2(tpyprz)_2][Mo_7O_{21}(O_3PCH_2PO_3)]\cdot 3.5H_2O$ (**9**·5H_2O), which contains a new heptamolybdate cluster $\{Mo_7O_{21}(O_3PCH_2PO_3)\}^{4-}$ and a cationic linear chain $\{Ni(tpyprz)\}_n^{4n+}$ substructure. The structural chemistry of the nickel–molybdophosphonate series contrasts with that of the corresponding copper–molybdophosphonate materials, reflecting in general the different coordination preferences of Ni(II) and Cu(II). Consequently, while the Cu(II)–organic complex building block of the copper family is invariably the binuclear $\{Cu_2(tpyprz)\}^{4+}$ subunit, the Ni(II) chemistry with tpyprz exhibits a distinct tendency toward catenation to provide $\{Ni_3(tpyprz)_2\}^{6+}$, $\{Ni_4(tpyprz)_3\}^{8+}$, and $\{Ni(tpyprz)\}_n^{4n+}$ building blocks as well as the common $\{Ni_2(tpyprz)\}^{4+}$ moiety. This results in a distinct structural chemistry for the nickel(II)–molybdophosphonate series with the exception of the methylenediphosphonate derivative **1** which is isostructural with the corresponding copper compound $[\{Cu_2(tpyprz)(H_2O)_2\}(Mo_3O_8)_2(O_3PCH_2PO_3)]$ (**2**). The structural chemistry of the nickel(II) series also reflects variability in the number of attachment sites at the molybdophosphonate clusters, in the extent of aqua ligation to the Ni(II) tpyprz subunit, and in the participation of phosphate oxygen atoms as well as molybdate oxo groups in linking to the nickel sites.

The vast compositional range, considerable structural diversity, extensive physical properties, and significant applications of inorganic oxides[1−4] have stimulated considerable interest in the rational design of new oxide materials. One approach to synthesis exploits organic building blocks which contribute to the structural complexity of the resultant hybrid material and which allow the combination of the unique characteristics of the organic and inorganic components in complementary roles to fashion new solid-state

* Author to whom correspondence should be addressed. E-mail: jazubiet@syr.edu.
[†] Syracuse University.
[‡] University of New Orleans.

(1) McCarroll, W. H. In *Encyclopedia of Inorganic Chemistry*; King, R. B., Ed.; John Wiley & Sons: New York, 1994; Vol. 6, pp 2903−2946.

10.1021/ic049201k CCC: $27.50
Published on Web 10/06/2004

architectures which exhibit composite or new physicochemical properties.[5−12]

An important subclass of these hybrid metal oxides is represented by the metal organophosphonates, which include complex molecular anions, as well as solid phases.[13,14] The protypical solid-state structure of these $M/O/(H_nO_3PR)^{(2-n)-}$ materials consists of M/O/P layers decorated on both surfaces by the organic groups R.[13] However, the structural variety exhibited by the molecular clusters of the oxovanadium− and oxomolybdenum−organophosphonate[15,16] families suggested that these polyoxoanions would serve as building blocks in the design of one-, two-, and three-dimensional materials. While this expectation was realized by exploiting the "venerable" polyoxomolybdates of the types $[Mo_5O_{15}(O_3PR)_2]^{4-}$ and $[Mo_6O_{18}(O_3AsR)_2]^{4-}$ as building blocks,[16−19] a secondary metal coordination complex cation was required to satisfy charge balance and space-filling considerations,[20−26] that is, charge density matching.[27] Consequently, it was recognized that, borrowing from the literature of metal organic frameworks (MOFs),[28−32] the molybdate cluster served as a node and, depending on the number of surface accessible linking sites, two- and three-dimensional materials would be isolated in the presence of appropriate secondary metals and binucleating ligands, as illustrated in Scheme 1. This three-component design strategy has been described by us in extensive investigations of the oxomolybdenum−organodiphosphonate/Cu(II)−organoimine and oxomolybdenum−organoarsonate/Cu(II)−organoimine systems. The structural determinants were readily identified as (i) the cluster volume which determines the number of accessible linkage sites on the surface of the metal oxide node, (ii) the identity of the ligand termini of the organic subunit, whether P or As, and (iii) the tether length of the organodiphosphonate subunit in that particular class. It is also apparent that the identity of the binucleating organoimine will profoundly influence the structure, for example, replacing tetra-2-pyridylpyrazine (tpyprz) with an extended tether such as 2,2′:4′,4″:2″,2‴-quarterpyridyl-6′,6″-di-2-pyridine (bis-terpy).[33] This aspect will be discussed in a future contribution.

(2) Bruce, D. W., O'Hare, D., Eds. *Inorganic Materials*, Wiley: Chichester, 1992.
(3) Cheetham, A. K. *Science* **1964**, *264*, 794.
(4) Cockayne, B., James, D. W., Eds. *Modern Oxide Materials*, Academic Press: New York, 1972.
(5) Stupp, S. I.; Braun, P. V. *Science*, **1997**, *277*, 1242 and references therein.
(6) Mitzi, D. B. *Prog. Inorg. Chem.* **1999**, *48*, 1.
(7) Hagrman, P. J.; Hagrman, D.; Zubieta, J. *Angew. Chem., Int. Ed. Engl.* **1999**, *38*, 2639.
(8) See for example: (a) Portier, J.; Choy, J.-H.; Subramamian, M. A. *Int. J. Inorg. Mater.* **2001**, *3*, 581. (b) Sanchez, C.; Soler-Illia, G. J. de A. A.; Ribot, F.; Lalot, T.; Mayer, C. R.; Calwil, V. *Chem. Mater.* **2001**, *13*, 3061 and references therein. (c) Sanchez, C., Ribot, F., Eds. *Proceedings of the First European Workshop on Hybrid Organic−Inorganic Materials.* Special issue of *New J. Chem.* **1994**, *18*. (d) Davis, M. E.; Katz, A.; Ahmad, W. R. *Chem. Mater.* **1996**, *8*, 1820. (e) Evans, O. R.; Ngo, L.; Lin, W. B. *J. Am. Chem. Soc.* **2001**, *123*, 10395. (f) Sawaki, T.; Aoyama, Y. *J. Am. Chem. Soc.* **1999**, *121*, 4793. (g) Abrahams, B. E.; Jackson, P. A.; Robson, R. *Angew. Chem., Int. Ed.* **1998**, *37*. 2656. (h) Li, H.; Eddaoudi, M.; O'Keeffe, M.; Yaghi, O. M. *Nature* **1999**, *402*, 276. (i) Blanford, C. F.; Do, T. N.; Holland, B. T.; Stein, A. *Mater. Res. Soc. Symp. Proc.* **1999**, *549*, 61. (j) Carlucci, L.; Ciani, G.; Moret, M.; Proserpio, D. M.; Rizzato, S. *Angew. Chem., Int. Ed.* **2000**, *39*, 1506. (k) Swift, J. A.; Ward, M. D. *Chem. Mater.* **2000**, *12*, 1501. (l) Chae, H. K.; Eddaoudi, M.; Kim, J.; Hauck, S. I.; Hartwig, J. F.; O'Keeffe, M.; Yaghi, O. M. *J. Am. Chem. Soc.* **2001**, *123*, 11482. (m) Zhao, H. R.; Heintz, A.; Ouyang, X.; Dunbar, K. R.; Campana, C. F.; Rogers, R. D. *Chem. Mater.* **1999**, *11*, 736.
(9) Forster, P. M.; Cheetham, A. K. *Top. Catal.* **2003**, *24*, 79−86.
(10) Clemente-Leon, M.; Coronado, E.; Gimenez-Saiz, C.; Gomez-Garcia, C. J. *NATO Sci. Ser., II: Mathematics, Physics and Chemistry* **2003**, *98*, 417−440.
(11) Clemente-Leon, M.; Coronado, E.; Gomez-Garcia, C. J.; Martinez-Ferrero, E. *J. Cluster Sci.* **2002**, *13*, 381−407.
(12) Robl, C. In *Chemistry at the Beginning of the Third Millennium: Molecular Design, Supramolecules, Nanotechnology and Beyond*, Proceedings of the German-Italian Meeting of Coimbra Group Universities, Pavia, Italy, Oct. 7−10, 1999; **2000**, 279−303.
(13) The chemistry of the metal organophosphonates has witnessed remarkable growth in the past decade. A number of useful reviews are available: (a) Clearfield, A. *Curr. Opin. Solid State Mater. Sci.* **2002**, *6*, 495. (b) Clearfield, A. *Prog. Inorg. Chem.* **1998**, *47*, 371. (c) Alberti, G. In *Comprehensive Supramolecular Chemistry;* Atwood, J. L., Davis, J. E. D., Vogel, F., Eds.; Pergamon Press: New York: 1996, Vol. 9, p 152. (d) Clearfield, A. In *Comprehensive Supramolecular Chemistry*, Atwood, J. L., Davies, J. E. D., Vogel, F., Eds.; Pergamon Press: New York, 1966; Vol. 9, p 107. (e) Clearfield, A. *Chem. Mater.* **1998**, *10*, 2801. (f) Vermeulen, L. A. *Prog. Inorg. Chem.* **1997**, *44*, 143.
(14) In addition to work referenced in these reviews, a wealth of new information on metal phosphonates has been published since the beginning of 2001. Some representative examples of novel results in this field include: (a) Tolis, E. I.; Helliwell, M.; Langley, S.; Raftery, J.; Winpenny, R. E. P. *Angew. Chem., Int. Ed.* **2003**, *42*, 3804. (b) Costantino, U.; Nocchetti, M.; Vivani, R. *J. Am. Chem. Soc.* **2002**, *124*, 8428. (c) Mao, J.-G.; Wang, Z.; Clearfield, A. *Inorg. Chem.* **2002**, *41*, 2334. (d) Arnold, D. I.; Ouyang, X.; Clearfield, A. *Chem. Mater.* **2002**, *14*, 2020. (e) Clearfield, A.; Sharma, C. V. K.; Zhang, B. *Chem. Mater.* **2001**, *13*, 3099. (f) Barthelet, K.; Merlier, C.; Serre, C.; Riou-Cavellec, M.; Riou, D.; Férey, G. *J. Mater. Chem.* **2002**, *12*, 1132. (g) Trobajo, C.; Khaisalsov, S. A.; Espina, A.; Garcia, J. R. *Chem. Mater.* **2001**, *13*, 4457. (h) Yin, P.; Zhang, L.-M.; Gao, S.; Xin, X.-Q. *Chem. Commun.* **2001**, 2346. (i) Hix, G. B.; Kariuki, B. M.; Kitchin, S.; Tremayne, M. *Inorg. Chem.* **2001**, *40*, 1477. (j) Odolul, F.; Bujoli, B.; Massiot, D. *Chem. Mater.* **2001**, *13*, 163. (k) Adair, B. A.; deDelgado, G. D.; Delgado, J. M.; Cheetham, A. K. *Solid State Sci.* **2000**, *2*, 119. (l) Neeraj, S.; Forster, P. M.; Rao, C. N. R.; Cheetham, A. K. *Chem. Commun.* **2001**, 2716. (m) Bellitto, C. In *Magnetism: Molecules to Materials II*; Miller, J. S., Drilles, M., Eds.; Wiley-VCH: Weinheim and New York, 2001; p 425. (n) Vioux, A.; Mutin, P.; Le Bideau, J.; Leclercq, D. Organophosphorus-Based Organic−Inorganic Hybrids. *Mater. Res. Soc. Sym. Proc.* **2001**, 628 (Organic/Inorganic Hybrid Materials, CC1.4.1-CC1.4.12.)
(15) Khan, M. I.; Zubieta, J. *Prog. Inorg. Chem.* **1995**, *43*, 1, and references therein.
(16) Chang, Y.-D.; Zubieta, J. *Inorg. Chim. Acta* **1996**, *245*, 177, and references therein.
(17) Kwak, W.; Pope, M. T.; Scully, T. F. *J. Am. Chem. Soc.* **1975**, *97*, 5735.
(18) Hedman, B. *Acta Crystallogr.* **1980**, *B36*, 2241.
(19) Kwak, W.; Rajkovic, L. M.; Stalick, J. K.; Pope, M. T.; Quicksall, C. O. *Inorg. Chem.* **1976**, *15*, 2778.
(20) Finn, R. C.; Zubieta, J. *Inorg. Chem.* **2001**, *40*, 2466.
(21) Burkholder, E.; Zubieta, J. *Chem. Commun.* **2001**, 2056−2057.
(22) Finn, R. C.; Burkholder, E.; Zubieta, J. *Chem. Commun.* **2001**, 1852−1853.
(23) Finn, R. C.; Rarig, R. S.; Zubieta, J. *Inorg. Chem.* **2002**, *41*, 2109.
(24) Burkholder, E.; Wright, S.; Golub, V.; O'Connor, C. J.; Zubieta, J. *Inorg. Chem.* **2003**, *42*, 7460−7471.
(25) Burkholder, E.; Golub, V.; O'Connor, C. J.; Zubieta, J. *Inorg. Chem.* **2003**, *42*, 6729−6740.
(26) Burkholder, E.; Golub, V.; O'Connor, C. J.; Zubieta, J. *Chem. Commun.* **2003**, 2128−2129.
(27) Maggard, P. A.; Boyle, P. D. *Inorg. Chem.* **2003**, *42*, 4250.
(28) Batten, S. R.; Robson, R. *Angew. Chem., Intl. Ed.* **1998**, *37*, 1461 and references therein.
(29) Sommerdijk, J. M. *Angew. Chem., Int. Ed.* **2003**, *42*, 3572 and references therein.
(30) Papaefstathiou, G. S.; MacGillivray, L. R. *Coord. Chem. Rev.* **2003**, *246*, 169.
(31) Rosi, N. L.; Eddaoudi, M.; Kim, J.; O'Keeffe, M.; Yaghi, O. M. *CrystEngComm*. **2002**, *4*, 401.
(32) Rosi, N. L.; Eddaoudi, M.; Kim, J.; O'Keeffe, M.; Yaghi, O. M. *Angew. Chem., Int. Ed.* **2002**, *41*, 284.

Scheme 1

A Modular Approach to the Design of Bimetallic Oxides: The Three Component System

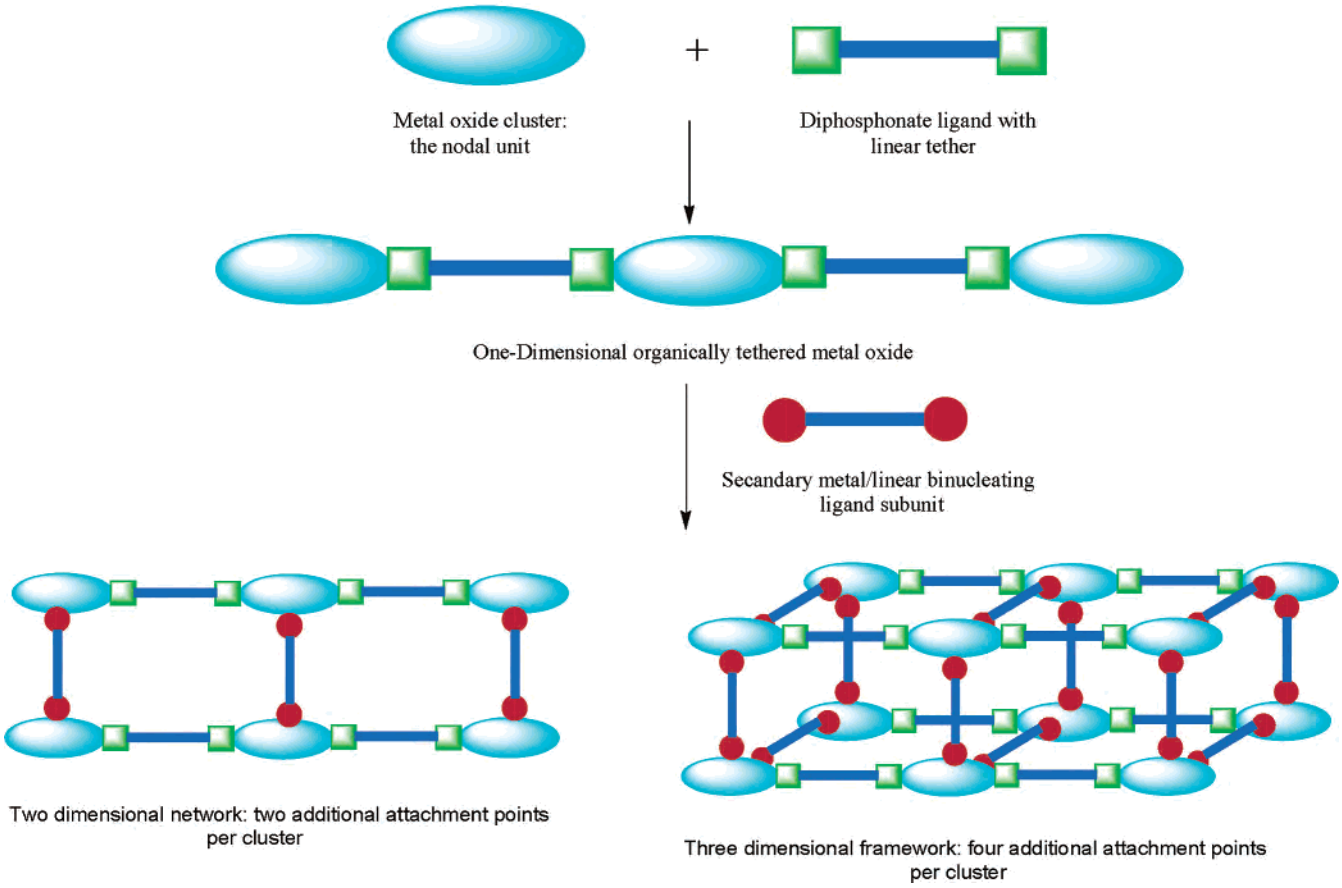

The identity of the secondary metal must also serve as a structural determinant, since the coordination preferences of different transition metal centers are quite distinct. Thus, our previous studies focused on Cu(II) as the secondary metal, a cation characterized by Jahn−Teller distortions from regular octahedral geometry and characteristically displaying square planar, "4 + 1," or "4 + 2" axially distorted coordination. These coordination preferences dictate that the Cu(II) center will most likely adopt $\{CuN_3L\}$, $\{CuN_3L_2\}$, or $\{CuN_3L_3\}$ coordination geometries with a meridional tridentate donor such as tpyprz, rather than assuming more regular $\{CuN_6\}$ by attaching to two tpyprz ligands and possibly catenating into $\{Cu_2(tpyprz)\}_n^{4n+}$ chains.[20−25] These distorted coordination modalities also afford the Cu(II) site considerable flexibility of attachment to the surface oxides of the cluster building block, a characteristic demonstrated in the structural variety observed for the oxomolybdate−organodiphosphonate/Cu(II)−tpyprz family.

In contrast, Ni(II) exhibits more regular six coordination, suggesting that the $\{NiN_6\}$ bonding pattern might effectively compete with the $\{NiN_3O_3\}$ coordination geometry required for linking the oxomolybdate−organodiphosphonate chains through $\{Ni_2(tpyprz)\}^{4+}$ subunits. Consequently, some degree of $\{Ni_x(tpyprz)_y\}_n$ catenation might be expected in the structural chemistry of the Ni(II) family. This possibility was realized in the preparation of the two-dimensional material $[\{Ni_4(tpyprz)_3\}\{Mo_5O_{15}(O_3PCH_2CH_2PO_3)\}_2]\cdot 23H_2O$.[26] It is noteworthy that while the corresponding Cu(II) containing material $[\{Cu_2(tpyprz)(H_2O)_2\}\{Mo_5O_{15}(O_3PCH_2CH_2PO_3)\}]$ exhibits the identical molybdophosphonate chain as the Ni-(II) material, the secondary metal−ligand subunits which serve to link these chains into the network architecture are quite distinct. In the case of Cu(II), the tpyprz ligand functions as a conventional dipodal rigid rod, that is, a binucleating linear ligand. In contrast, the Ni(II)−tpyprz substructure consists of a tetranuclear linear cluster, $\{Ni_4(tpyprz)_3\}^{8+}$, with two distinct Ni(II) environments and an attachment mode to the molybdophosphonate chains which results in a distinct ruffling of the network, a feature which in turn produces significant interlamellar cavities to accommodate a significant amount of water of crystallization (11.4% by mass). The profound structural differences between $[\{Cu_2(tpyprz)(H_2O)_2\}\{Mo_5O_{15}(O_3PCH_2CH_2PO_5)\}]$ and $[\{Ni_4(tpyprz)_3\}\{Mo_5O_{15}\ (O_3PCH_2CH_2PO_3)\}_2]\cdot 23H_2O$ suggested that the parallel study of the Ni(II) family, oxomolybdenum−diphosphonate/Ni(II)−tpyprz, would reveal the structural consequences of Ni(II) substitution for Cu(II) as the tether length of the organodiphosphonate,

(33) Koo, B.-K.; Ouellette, W.; Burkholder, E. M.; Golub, V.; O'Connor, C. J.; Zubieta, J. *Solid State Sci.* **2004**, *6*, 461.

$[H_nO_3P(CH_2)_xPO_3H_m]^{(4-n-m)-}$ ($x = 1-5$), was varied. Indeed, the structural characteristics of the nickel family are quite distinct from those of the corresponding members of the copper series. Only in the case of the methylenediphosphonate compounds are isomorphous structures observed. Thus, $[\{Ni_2(tpyprz)(H_2O)_2\}(Mo_3O_8)_2(O_3PCH_2PO_3)_2]$ (**1**) and $[\{Cu_2(tpyprz)(H_2O)_2\}(Mo_3O_8)_2(O_3PCH_2PO_3)_2]$ (**2**) exhibit the same three-dimensional structure. The compounds $[\{Ni_4(tpyprz)_3\}\{Mo_5O_{15}(O_3PCH_2CH_2PO_3)\}_2]\cdot 2\cdot 3H_2O$ (**3**$\cdot 23H_2O$) and $[\{Ni_3(tpyprz)_2(H_2O)_2\}(Mo_5O_{15})(Mo_2O_4F_2)\{O_3P(CH_2)_3PO_3\}_2]\cdot 8H_2O$ (**5**$\cdot 8H_2O$) are two-dimensional but structurally unique when compared to the Cu(II) analogues. The materials $[\{Ni_2(tpyprz)_2\}Mo_5O_{15}\{O_3P(CH_2)_4PO_3\}]\cdot 6.65H_2O$ (**6**$\cdot 6.65H_2O$) and $[\{Ni_2(tpyprz)_2\}Mo_5O_{15}\{O_3P(CH_2)_5PO_3\}]\cdot 3.75H_2O$ (**8**$\cdot 3.75H_2O$), are one-dimensional, while $[\{Ni_2(tpyprz)(H_2O)_3\}Mo_5O_{15}\{O_3P(CH_2)_3PO_3\}]\cdot H_2O$ (**4**$\cdot H_2O$) and $[\{Ni_2(tpyprz)(H_2O)_2\}Mo_5O_{15}\{O_3P(CH_2)_4PO_3\}]\cdot 2.25H_2O$ (**7**$\cdot 2.25H_2O$) are three-dimensional. Two compounds, $[Ni_2(tpyprz)_2][Mo_7O_{21}(O_3PCH_2PO_3)]\cdot 3.5H_2O$ (**9**$\cdot 3.5H_2O$) and $[Ni_2(tpyprz)_2][Mo_6O_{18}(H_2O)(O_3PC_6H_5)_2]\cdot 6.4H_2O$ (**10**$\cdot 6.4H_2O$), consist of molecular anions and one-dimensional $\{Ni(tpyprz)\}_n^{2n+}$ chains.

Experimental Section

Materials and General Procedures. Chemicals were used as obtained without further purification with the exception of the diphosphonic acids ($n = 3-5$), which were synthesized by slight modification of the reported methods.[34−36] Ammonium molybdate(VI) tetrahydrate and tetra-2-pyridinylpyrazine (tpyprz) were purchased from Aldrich; nickel(II) acetate tetrahydrate, nickel(II) nitrate hexahydrate, nickel(II) sulfate hexahydrate, copper(II) acetate monohydrate, hydrofluoric acid (41−51% HF), acetic acid, molybdenum(VI) oxide 99.5%, methylenediphosphonic acid, phenylphosphonic acid, and 1,2-ethylenediphosphonic acid were purchased from Alfa Aesar. All syntheses were carried out in 23 mL poly(tetrafluoroethylene) lined stainless steel containers under autogenous pressure. The reactants were stirred briefly, and the initial pH was measured before heating. Water was distilled above 3.0 MΩ in-house using a Barnstead model 525 Biopure distilled water center. The initial and final pH of each reaction were measured using color pHast sticks. Infrared spectra were obtained on a Perkin-Elmer 1600 series FTIR spectrometer.

Synthesis of $[\{Ni_2(tpyprz)(H_2O)_2\}\{Mo_3O_8(O_3PCH_2PO_3)\}_2]$ (1). The reaction of $(NH_4)_6Mo_7O_{24}\cdot 4H_2O$ (0.132 g, 0.107 mmol), $Ni(CH_3CO_2)_2\cdot 4H_2O$ (0.073 g, 0.293 mmol), tpyprz (0.087 g, 0.224 mmol), $H_2PO_3CH_2PO_3H_2$ (0.057 g, 0.452 mmol), H_2O (10.037 g, 556 mmol), and HF (0.127 g) in the mole ratio 0.48:1.31:1.00:2.02:2486 at 200 °C for 144 h yielded orange crystals of **1** in 72% yield which were suitable for X-ray diffraction. pH: initial, 2.0; final, 1.5. IR (KBr pellet, cm^{-1}): 3854(m), 3650(m), 3431(w), 1647(s), 1458(m), 1410(m), 1151(m), 1119(s), 1081(s), 1026(s), 942(s), 839(s), 789(s), 672(s), 581(w), 540(m).

Synthesis of $[\{Cu_2(tpyprz)(H_2O)_2\}\{Mo_3O_8(O_3PCH_2PO_3)\}_2]$ (2). A solution of MoO_3 (0.176 g, 1.223 mmol), $Cu(CH_3CO_2)_2\cdot H_2O$ (0.100 g, 0.501 mmol), tpyprz (0.086 g, 0.221 mmol), $H_2PO_3CH_2PO_3H_2$ (0.109 g, 0.865 mmol), H_2O (10.202 g, 566 mmol), and CH_3CO_2H (0.210 g) in the mole ratio 5.53:2.27:1.00:3.91:2561 at 200 °C for 48 h yielded dark green crystals of **2** in 40% yield. The initial and final pH were 1.5 and 2.0, respectively. IR (KBr pellet, cm^{-1}): 3461(m), 1637(w), 1598 (w), 1474(w), 1413(w), 1258(w), 1198(w), 1152(s), 1123(s), 1086(s), 1030(s), 935(s), 907-(s), 894(s), 789(s), 676(s), 576(m), 538(m).

Synthesis of $[\{Ni_4(tpyprz)_3\}\{Mo_5O_{15}(O_3PCH_2CH_2PO_3)\}_2]\cdot 23H_2O$ (3·23H$_2$O). The reaction of MoO_3 (0.160 g, 1.112 mmol), $Ni(CH_3CO_2)_2\cdot 4H_2O$ (0.110 g, 0.442 mmol), tpyprz (0.086 g, 0.221 mmol), $H_2PO_3(CH_2)_2PO_3H_2$ (0.084 g, 0.442 mmol), H_2O (10.03 g, 557 mmol), and HF (0.123 g, 3.07 mmol) in the mole ratio 5.03:2.00:1.00:2.00:2520:13.89 at 200 °C for 96 h provided orange crystals of **3**$\cdot 23H_2O$ in 25% yield based on Mo which were suitable for X-ray diffraction. pH: initial, 1.5; final, 1.0. IR (KBr pellet, cm^{-1}): 3422(s), 1701(w), 1636(w), 1597(w), 1476(w), 1414(m), 1306(w), 1200(w), 1129(m), 1064(m), 1046(m), 936(m), 918(s), 894(s), 770(m), 699(s), 560(m), 532(m), 424(w).

Synthesis of $[\{Ni_2(tpyprz)_2(H_2O)_3\}Mo_5O_{15}\{O_3P(CH_2)_3PO_3\}]\cdot H_2O$ (4·H$_2$O). A solution of $(NH_4)_6Mo_7O_{24}\cdot 4H_2O$ (0.195 g, 0.158 mmol), $Ni(NO_3)_2\cdot 6H_2O$ (0.128 g, 0.440 mmol), tpyprz (0.086 g, 0.221 mmol), $H_2PO_3(CH_2)_3PO_3H_2$ (0.089 g, 0.436 mmol), H_2O (10.048 g, 558 mmol), and HF (0.146 g) was placed in an 200 °C oven for 96 h in the mole ratio 0.72:1.99:1.00:1.97:2525. Two types of crystals were generated. The first phase of crystals was pale yellow rods in a 25% yield, and the second phase of crystals was orange blocks in 65% yield, corresponding to compound **3**$\cdot H_2O$ and **4**$\cdot 8H_2O$, respectively. pH: initial, 1.5; final, 1.5. IR (KBr pellet, cm^{-1}): 3144(w), 1654(w), 1595(m), 1471(m), 1406(m), 1236(w), 1198(w), 1140(s), 1100(s), 1027(s), 1004(w), 971(s), 919(s), 894-(s), 855(s), 788(m), 761(w), 675(s), 582(m), 540(m), 426(m).

Synthesis of $[\{Ni_3(tpyprz)_2(H_2O)_2\}\{Mo_5O_{15}\}\{Mo_2F_2O_4\}\{O_3P(CH_2)_3PO_3\}_2]\cdot 8H_2O$ (5·8H$_2$O). A solution of $(NH_4)_6Mo_7O_{24}\cdot 4H_2O$ (0.196 g, 0.159 mmol), $NiSO_4\cdot 6H_2O$ (0.118 g, 0.449 mmol), tpyprz (0.087 g, 0.224 mmol), $H_2PO_3(CH_2)_3PO_3H_2$ (0.092 g, 0.451 mmol), H_2O (10.040 g, 557 mmol), and HF (0.144 g) in the mole ratio 0.71:2.00:1.00:2.01:2487 was stirred briefly before heating to 200 °C for 96 h. pH: initial, 1.5; final, 2.0. Orange blocks of **4**$\cdot 8H_2O$, suitable for X-ray diffraction, were isolated in 80% yield. IR (KBr pellet, cm^{-1}): 3384(w), 1599(w), 1475(w), 1418(w), 1217(w), 1156(m), 1017(m), 956(s), 927(s), 899(s), 782(w), 689(s), 564(m), 510(w).

Synthesis of $[\{Ni_2(tpyprz)_2\}Mo_5O_{15}\{O_3P(CH_2)_4PO_3\}]\cdot 6.65H_2O$ (6·6.65H$_2$O). A solution of $(NH_4)_6Mo_7O_{24}\cdot 4H_2O$ (0.131 g, 0.106 mmol), $Ni(CH_3CO_2)_2\cdot 4H_2O$ (0.072 g, 0.289 mmol), tpyprz (0.087 g, 0.224 mmol), $H_2PO_3(CH_2)_4PO_3H_2$ (0.099 g, 0.454 mmol), H_2O (10.020 g, 556 mmol), and HF (0.159 g) in the mole ratio 0.47:1.29:1.00:2.03:2482 was heated to 200 °C for 96 h. Orange crystals of **5**$\cdot 6.65H_2O$ were isolated in a 20% yield. pH: initial, 1.5; final, 1.5. IR (KBr pellet, cm^{-1}): 3443(s) 3071(w), 1633(w), 1597(m), 1465(m), 1403(m), 1303(w), 1204(w), 1040(w), 971(m), 929(s), 902(s), 890(m), 788(m), 703(s), 576(w), 562(w), 532(w).

$[\{Ni_2(tpyprz)(H_2O)_2\}Mo_5O_{15}\{O_3P(CH_2)_4PO_3\}]\cdot 2.25H_2O$ (7·2.25H$_2$O). A mixture of $(NH_4)_6Mo_7O_{24}\cdot 4H_2O$ (0.195 g 0.158 mmol), $NiSO_4\cdot 6H_2O$ (0.116 g, 0.441 mmol), tpyprz (0.085 g, 0.219 mmol), $H_2PO_3(CH_2)_4PO_3H_2$ (0.096 g, 0.440 mmol), H_2O (10.040 g, 557 mmol), and HF (0.150 g) in the mole ratio 0.72:2.01:1.00:2.01:2543 was stirred briefly before heating to 200 °C. pH: initial, 1.5; final, 2.0. Green crystals of **6**$\cdot 2.25H_2O$, in a 65% yield, were isolated after 96 h. IR for **6**$\cdot 2.25H_2O$ (KBr pellet, cm^{-1}): 3345-(m), 1601(w), 1478(w), 1910(m), 1389(w), 1211(w), 1163(w), 1113(m), 1047(m), 981(m), 935(s), 904(s), 852(s), 784(m), 676-(s), 581(w).

Synthesis of $[\{Ni_2(tpyprz)_2\}Mo_5O_{15}\{O_3P(CH_2)_5PO_3\}]\cdot 3.75H_2O$ (8·3.75H$_2$O). A solution of $(NH_4)_6Mo_7O_{24}\cdot 4H_2O$ (0.197 g, 0.159

(34) McKenna, C. E.; Higa, M. T.; Cheung, N. H.; McKenna, M. C. *Tetrahedron Lett.* **1977**, 155−8.
(35) Wang, Z.; Heising, J. M.; Clearfield, A. *J. Am. Chem. Soc.* **2003**, *125*, 10375−10383.
(36) Arnold, D. I.; Ouyang, X.; Clearfield, A. *Chem. Mater.* **2002**, *14*, 2020−2027.

mmol), $Ni(NO_3)_2 \cdot 6H_2O$ (0.128 g, 0.440 mmol), tpyprz (0.086 g, 0.221 mmol), $H_2PO_3(CH_2)_5PO_3H_2$ (0.106 g, 0.457 mmol), H_2O (10.048 g, 558 mmol), and HF (0.155 g) in the mole ratio 0.72:1.99:1.00:2.07:2525 was stirred before heating to 200 °C for 96 h. Orange crystals of **7**·3.75H_2O were isolated in 45% yield. pH: initial, 1.5; final, 1.5. IR (KBr pellet, cm^{-1}): 3421(w), 1647(m), 1594(w), 1458(w), 1400(m), 1304(w), 1204(w), 1148(w), 1105(m), 1074(w), 979(m), 924(s), 899(s), 856(w), 791(w), 685(s), 563(m), 420(w).

Synthesis of $[Ni_2(tpyprz)_2][Mo_7O_{21}(O_3PCH_2PO_3)]\cdot 3.5H_2O$ (9·3.5H_2O). A reaction mixture of $(NH_4)_6Mo_7O_{24}\cdot 4H_2O$ (0.134 g, 0.108 mmol), $Ni(CH_3CO_2)_2\cdot 4H_2O$ (0.123 g, 0.494 mmol), tpyprz (0.098 g, 0.252 mmol), $H_2O_3PCH_2PO_3H_2$ (0.077 g, 0.611 mmol), H_2O (10.034 g, 557 mmol), and CH_3CO_2H (0.217 g) in the mole ratio 0.43:1.96:1.00:2.42:2210 was heated to 180 °C for 144 h. Hexagonal orange crystals were isolated in 85% yield. pH: initial, 4.0; final, 4.0. IR (KBr pellet, cm^{-1}): 3444(w), 1647(m), 1594(w), 1476(w), 1406(m), 1199(m), 1159(m), 1109(w), 1045(m), 1015(m), 935(s), 895(s), 809(m), 786(s), 748(s), 669(s), 565(w), 534(w), 419(w).

Synthesis of $[Ni_2(tpytrz)_2][Mo_6O_{18}(H_2O)(O_3PC_6H_5)_2]\cdot 6.4H_2O$ (10·6.4H_2O). A mixture of $(NH_4)_6Mo_7O_{24}\cdot 4H_2O$ (0.130 g, 0.105 mmol), $Ni(CH_3CO_2)_2\cdot 4H_2O$ (0.073 g, 0.293 mmol), tpyprz (0.086 g, 0.221 mmol), $C_6H_5PO_3H_2$ (0.140 g, 0.886 mmol), H_2O (10.003 g, 555 mmol), and HF (0.130 g) in the mole ratio 0.48:1.33:1.00:4.01:2511 at 200 °C for 96 h yielded orange crystal of **9**·6.4H_2O in 40% yield. pH: initial, 1.5; pH: 1.5. IR (KBr pellet, cm^{-1}): 3448(w), 1647(m), 1474(w), 1420(w), 1212(w), 1081(m), 1016(w), 963(m), 906(s), 786(m), 693(s), 564(w) and 529(w).

X-ray Crystallography. Structural measurements for **1**−**10** were performed on a Bruker-AXS SMART-CCD diffractometer at low temperature (90 K) using graphite-monochromated Mo Kα radiation ($\lambda_{Mo\ K_\alpha} = 0.71073$ Å).[37] The data were corrected for Lorentz and polarization effects and absorption using SADABS.[38] The structures were solved by direct methods. All non-hydrogen atoms were refined anisotropically. After all of the non-hydrogen atoms were located, the models were refined against F^2 initially using isotropic and later anisotropic thermal displacement parameters. Hydrogen atoms were introduced in calculated positions and refined isotropically. Neutral atom scattering coefficients and anomalous dispersion corrections were taken from the *International Tables*, Vol. C. All calculations were performed using SHELXTL crystallographic software packages.[39]

Crystallographic details for structure **1**−**10** are summarized in Table 1. Space group assignments and structure solutions and refinements were unexceptional except for compounds **4**·H_2O, **9**·3.5H_2O, and **10**·6.4H_2O. Compound **4**·H_2O was determined to be nonmerohedrally twinned from the initial diffraction pattern. The program Cell_Now [40] indicated that compound **4**·H_2O was composed of two crystal domains with the second domain rotated by 180° with respect to the first crystal domain. A twin law was created and imported into SAINT-Plus software package [41] where the data were corrected for Lorentz and polarization effects and absorption using TWINABS.[42] The structure was then solved by direct methods and refined by the conventional methodology.

Table 1. Summary of Crystallographic Data

	1	**2**	**3**·2.23H_2O	**4**·H_2O	**5**·8H_2O	**6**·6.65H_2O	**7**·2.25H_2O	**8**·3.75H_2O	**9**·3.5H_2O	**10**·6.4H_2O
emprical formula	$C_{13}H_{12}N_3Ni$-$Mo_3O_{15}P_2$	$C_{13}H_{12}N_3Cu$-$Mo_3O_{15}P_2$	$C_{38}H_{51}N_9Ni_2$-$Mo_5O_{32.5}P_2$	$C_{27}H_{30}N_6Ni_2$-$Mo_5O_{25}P_2$	$C_{108}H_{120.30}N_{24}Ni_6$-$Mo_{14}O_{78.15}P_8F_4$	$C_{52}H_{53.3}N_{12}Ni_2$-$Mo_5O_{27.65}P_2$	$C_{28}H_{32.5}N_6Ni_2$-$Mo_5O_{25.50}P_2$	$C_{53}H_{49.50}N_{12}Ni_2$-$Mo_5O_{24.75}P_2$	$C_{49}H_{41}N_{12}Ni_2$-$Mo_7O_{30.5}P_2$	$C_{60}H_{56.75}N_{12}Ni_2$-$Mo_6O_{31.5}P_2$
fw	858.73	863.56	1813.01	1497.63	5024.16	1947.83	1520.16	1909.61	2136.88	2204.92
cryst syst	triclinic	triclinic	orthorhombic	triclinic	monoclinic	monoclinic	triclinic	monoclinic	monoclinic	orthorhombic
space group	$P\bar{1}$	$P\bar{1}$	*Pbca*	$P\bar{1}$	$P2_1/n$	$P2_1/n$	$P\bar{1}$	$P2_1/n$	*Cc*	$Pna2_1$
a, Å	9.6676(5)	9.6137(6)	24.674(1)	8.704(2)	16.1269(7)	16.2142(6)	12.4451(6)	16.075(1)	11.806(1)	24.8493(9)
b, Å	11.0988(5)	11.3905(7)	15.4148(8)	10.769(2)	36.997(2)	16.8347(6)	12.9157(7)	17.326(1)	24.057(3)	13.2818(5)
c, Å	11.5999(6)	11.5527(7)	30.813(2)	22.068(4)	25.332(1)	23.7990(9)	13.4289(7)	23.249(2)	22.381(3)	21.6657(8)
α, deg	70.135(1)	70.774(1)	90	88.90(3)	90	90	96.827(1)	90	90	90
β, deg	75.460(1)	74.806(1)	90	86.66(3)	96.716(1)	104.605(1)	99.047(1)	103.316(1)	99.901(2)	90
γ, deg	70.887(1)	70.495(1)	90	80.23(3)	90	90	92.302(1)	90	90	90
V, Å	1092.29(9)	1109.4(1)	11719(1)	2035.0(70	15010.8(1)	6286.3(4)	2112.7(2)	6300.9(8)	6261.5(1)	7150.6(5)
Z	2	2	8	2	4	4	2	4	4	4
D_{calcd}, g cm^{-3}	2.611	2.585	2.053	2.444	2.224	2.058	2.390	2.013	2.267	2.048
μ, mm^{-1}	2.764	2.831	1.821	2.577	2.058	1.701	2.485	1.691	2.094	1.675
T, K	90(2)	90(2)	90(2)	90(2)	90(2)	90(2)	90(2)	90(2)	90(2)	90(2)
λ, Å	0.71073	0.71073	0.71073	0.71073	0.71073	0.71073	0.71073	0.71073	0.71073	0.71073
R_1[a](all data)	0.0269	0.0316	0.0849	0.0898	0.0892	0.0548	0.0327	0.0686	0.0766	0.0803
wR_2[b](all data)	0.0580	0.0671	0.1179	0.1405	0.1270	0.0987	0.0764	0.1495	0.1113	0.1217
flack									0.00(8)	0.0(3)

[a] $R_1 = \Sigma||F_o| - |F_c||/\Sigma|F_o|$. [b] $wR_2 = \{\Sigma[w(F_o^2 - F_c^2)^2]/\Sigma[w(F_o^2)^2]\}^{1/2}$.

(37) Bruker-AXS. *SMART Software,* Version 5.630; Siemens Analytical X-ray Instruments, Inc.: Madison, WI, USA, 1994.

(38) Sheldrick, G. M. *SADABS: Program for Empirical Absorption Corrections;* University of Göttingen: Göttingen, Germany, 1996.

(39) Sheldrick, G. M. *SHELXTL-Plus: Program for Refinement of Crystal Structures;* Version 6.14. Bruker-AXS: Madison, WI, USA, 1996.

(40) Sheldrick, G. M. *Cell_Now,* 1-22-2004; Bruker-AXS: Göttingen, Germany, 2004.

(41) Sheldrick, G. M. *SAINT-Plus,* Version 6.45; Bruker-AXS: Madison, WI, USA, 1996.

Compounds **9**·3.5H_2O and **10**·6.4H_2O are both acentric. Absences and reflection symmetry were consistent with the centric *C*2/*m* and the acentric *C*2 space groups for **9**·3.5H_2O. Since no satisfactory refinement could be obtained in the *C*2/*m*, the acentric choice was pursued. In the case of **10**·6.4H_2O, the space group was unambiguously determined to be $Pna2_1$.

Atomic positional parameters, full tables of bond lengths and angles, and anisotropic temperature factors are available in the Supporting Material. Selected bond lengths and angles for **1**−**10** are given in Table 1.

Magnetism. Magnetic data were recorded on 17−25 mg samples of compound in the 2−300 K temperature range using a Quantum Design MPMS-5S SQUID spectrometer. Calibrating and operating procedures have been reported previously[43]. The temperature-dependent data were obtained at a magnetic field of $H = 1000$ Oe.

Thermal Gravimetric Analyses. Thermogravimetric studies were preformed using 10−25 mg samples in an Auto TGA 2950 instrument under a 50 mL/min flow of synthetic air. The temperature was ramped from 25 to 650 °C at a rate of 5 °C/min for the decomposition.

Thermodiffraction. Thermodiffraction data were collected on a Bruker-AXS D8 Advance automated diffractometer equipped with a TTK 450 heating stage using Cu Kα radiation. The powder was placed in the sample holder, which acted as the heating system. The step size was 0.02° in 2θ, and the heating rate from room temperature to 275 °C was 0.5 °C/s and 0.2 °C/s for the temperature range 300 to 425 °C. The delay time between reaching the set temperature and measuring the diffraction pattern was 5 min. All temperature spectra were collected under vacuum.

Results and Discussion

Synthesis and Infrared Spectroscopy. The bimetallic oxides of this study were prepared by conventional hydrothermal methods,[44−46] which, as we and others have noted, provide ideal conditions for solubilizing and crystallizing organic/inorganic hybrid materials.[47] For compounds **1** and **3**−**10**, the reaction mixtures consisted of a molybdate source, $(NH_4)_6Mo_7O_{24}$·4H_2O or MoO_3, a Ni(II) salt, tetra-2-pyridinylpyrazine (tpyprz), the organophosphonate, and HF, which serves to solubilize the oxide starting materials and as a mineralizer.[44] While fluoride is generally not incorporated into the molybdenum oxide products, oxyfluorinated products are well-established for the hybrid materials of the vanadium oxide family[48,49] and have been encountered for the molybdenum oxides on occasion.[50] Curiously, fluoride uptake occurs only in the case of **5**·8H_2O, which is isolated in a mixture with **4**·H_2O when $Ni(NO_3)_2$·6H_2O is used as the NI-(II) source. However, when $NiSO_4$·6H_2O is used as the starting material, **5**·8H_2O is obtained as a monophasic, crystalline solid.

While hydrothermal parameter space was not explored exhaustively, optimization studies indicated that initial pH in the range 1.5−2.5 and temperatures of ca. 200 °C provided the most satisfactory results. Satisfactory crystal growth required the presence of HF, as only microcrystalline products were obtained in its absence. Similarly, product yields and crystallinity were highly dependent on the Ni(II) source, such that $Ni(NO_3)_2$·6H_2O, $Ni(SO_4)$·6H_2O, and $Ni(CH_3CO_2)_2$·4H_2O gave dramatically different yields of products under similar conditions and stoichiometrics with a particular organophosphonate.

In an attempt to produce an analogous Cu(II) phase, the reaction of MoO_3 with tpyprz, $H_2O_3PCH_2PO_3H_2$, and $Cu(CH_3CO_2)_2$·H_2O was also carried out. In this case, CH_3CO_2H was required to adjust the pH to 1.5. The product **2** was found to be isomorphous to **1**. It is noteworthy that this is the only case of isostructural pairs for the Ni(II) and Cu(II) families of oxomolybdenum−organophosphonate/M(II)−tpyprz materials.

The infrared spectra of **1**−**10** exhibit two strong bands in the 850−940 cm^{-1}, region attributed to symmetric and antisymmetric υ(Mo═O) of the cis $\{MoO_2\}$ units of the structures and medium to strong bands in the 675 to 740 cm^{-1} range, associated with υ(Mo−O−Mo). A series of two or three medium to strong peaks in the 960−1160 cm^{-1} range are attributed to υ(P−O) bands of the organophosphonate ligands, while the prominent bands in the 1400−1650 cm^{-1} region are assigned to the tpyprz ligand.

X-ray Structures. In common with the oxomolybdate−organophosphonate/Cu(II)−tpyprz materials reported previously, the structural chemistry of the oxomolybdate−organophosphonate/Ni(II)−tpyprz family of this study exhibits an unusual variety of structural motifs, reflected in one-, two-, and three-dimensional materials, as well as molecular clusters. However, in contrast to the Cu(II) class where the cationic component is exclusively $\{Cu_2(tpyprz)(H_2O)_x\}^{4+}$, the consequences of the different coordination preferences of Ni-(II) are manifested in the incorporation of oligomeric or one-dimensional $\{Ni_x(tpyprz)_y\}_n^{2x+}$ building blocks, containing $\{NiN_6\}$ cores as well as the more common $\{NiN_3O_3\}$ coordination mode. Consequently, a variety of novel building blocks are encountered in the structural chemistry.

The simplest structures contain molecular oxomolybdate−organophosphonate subunits and are represented by $[Ni_2(tpyprz)_2][Mo_7O_{21}(O_3PCH_2PO_3)]$·3.5$H_2O$ (**9**·3.5H_2O) and $[Ni_2(tpyprz)_2][Mo_6O_{18}(H_2O)(O_3PC_6H_5)_2]$·6.4$H_2O$ (**10**·6.4H_2O). As illustrated in Figure 1, the structure of **10** consists of discrete $\{Mo_6O_{18}(H_2O)(O_3PC_6H_5)_2\}^{4-}$ molecular anions, embedded in a matrix of one-dimensional $\{Ni(tpyprz)\}_n^{4n+}$ chains. The molecular anion consists of a ring of five molybdenum octahedra and one square pyramid capped on either pole by $\{O_3PC_6H_5\}^{2-}$ tetrahedra. While an analogous organoarsonate $[Mo_6O_{18}(H_2O)(O_3AsC_6H_5)_2]^{4-}$ [51] has been reported, the structures are distinct in detail. The arsonate consists of a ring of molybdate octahedra with two polyhedra

(42) Sheldrick, G. M. *TWINABS: Program for the Empirical Absorption Corrections for Twins;* Bruker-AXS: Madison, WI, USA, 2003.
(43) O'Connor Charles, J. *Prog. Inorg. Chem.* **1979**, *29*, 203−283.
(44) Laudise, R. A. *Chem. Eng. News* **1987**, *65*, 30.
(45) Lobachev, A. N. *Crystallization Processes Under Hydrothermal Conditions*; Consultants Bureau: New York, 1973.
(46) Gopalakrishnan, J. *Chem. Mater.* ***1995***, *7*, 1265.
(47) Zubieta, J. Solid-State Methods, Hydrothermal In *Comp. Coord. Chem. II* **2004**, *1*, 697−709.
(48) Riou, D.; Ferey, G. *J. Solid State Chem.* **1994**, *111*, 422.
(49) Ninclaus, C.; Riou, D.; Ferey, G. *Chem. Commun.* **1997**, 851.
(50) Burkholder, E.; Zubieta, J. *Inorg. Chim. Acta* **2004**, *357*, 279.
(51) Kwak, W.; Rajkovic, L. M.; Pope, M. T.; Quicksall, C. O.; Matsumoto, K. Y.; Sasaki, Y. *J. Am. Chem. Soc.* **1977**, *99*, 6463.

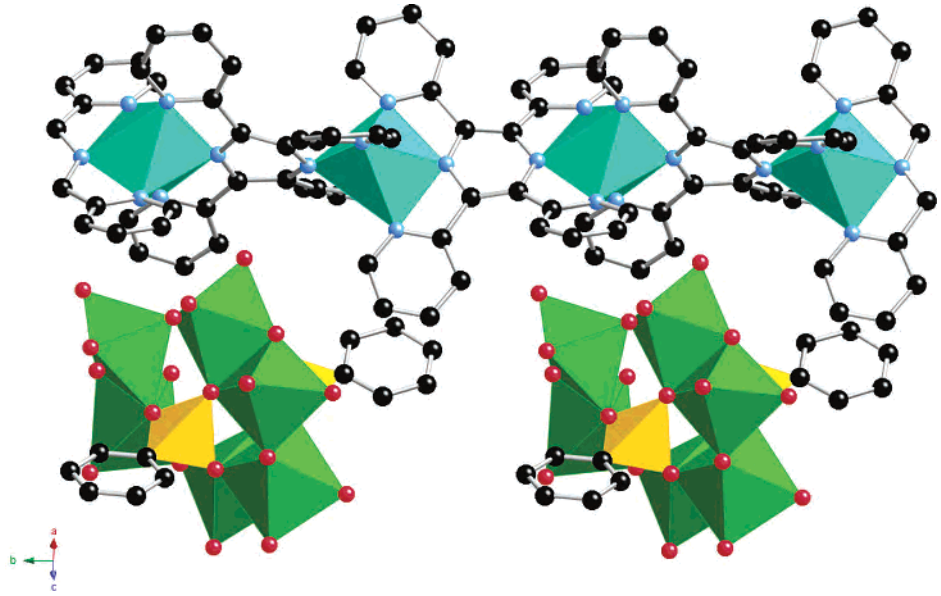

Figure 1. A polyhedral representation of the structure of $[Ni_2(tpyprz)_2][Mo_6O_{18}(H_2O)(O_3PC_6H_5)_2]\cdot 6.4H_2O$ (**10**·$6.4H_2O$): molybdenum polyhedra, green; nickel octahedra, blue; phosphorus tetrahedra, yellow; oxygen atom, red spheres; nitrogen, light blue spheres; carbon, black spheres.

exhibiting a face-sharing interaction through two oxo groups and the aqua ligand. In contrast, the anion of **10** features a trigonal bipyramidal site and a terminal aqua ligand. Curiously, the structure of **10** does not contain the common $\{Mo_5O_{15}(O_3PR)_2\}^{4-}$ cluster as a constituent, since this is the dominant form under these reaction conditions. The latter observation is illustrated in the Cu(II) chemistry, where the pentamolybdate cluster serves as a building block in the structure of $[\{Cu_2(tpyprz)(H_2O)\}Mo_5O_{15}(O_3PC_6H_5)_2]$ (Table 2).

The Ni(II)−tpyprz chain consists of octahedral $\{NiN_6\}$ sites linked through the carbon backbones of the tpyprz ligands. Each Ni(II) site bonds in a meridional arrangement to two pyridyl donors and one pyrazine nitrogen donor of adjacent tpyprz ligands. The coordination geometry is quite regular with an Ni−N pyridyl average bond length of 2.048(6) Å (range 1.996−2.095 Å) and an Ni−N pyrazine average bond length of 2.106(6) Å (range 2.095−2.117 Å). The catenation is likely a reflection of the preference of Ni(II) to adopt more regular octahedral geometry than that of Cu(II) and the modestly reduced oxophilicity of Ni(II) in comparison to that of Cu(II).

The structure of $[Ni_2(tpyprz)_2][Mo_7O_{21}(O_3PCH_2PO_3)]\cdot 3.5H_2O$ (**9**·$3.5H_2O$) also consists of molecular anions and $\{Ni(tpyprz)\}_n^{2n+}$ chains. As shown in Figure 2, the structure of the molecular anion is constructed from five molybdenum octahedra and two square pyramids in a corner- and edge-sharing arrangement which forms a hollow occupied by the methylenediphosphonate ligand. As noted previously,[52,53] methylenediphosphonate does not possess sufficient extension to bridge cluster building blocks and preferentially forms six membered [−M−O−P−C−P−O−] chelate rings through the oxygen atoms of either phosphate terminus. The diphosphonate oxygen donors are exclusively associated with the five and six coordinate molybdenum sites, providing three {P−O−Mo} linkages and two $\{P-O-Mo_2\}$ bonds; one phosphonate oxygen is pendant and multiply bonded to the phosphorus {P═O}, hence not protonated. The cluster represents a new member of the oxomolybdophosphonate polyanion family.

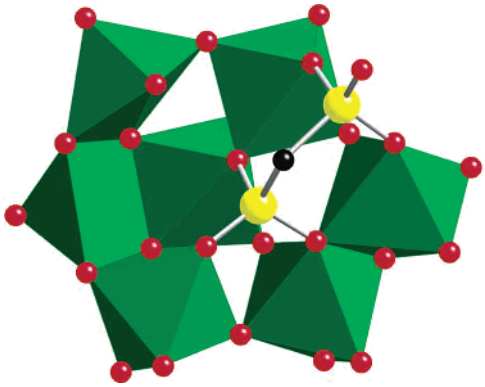

Figure 2. A view of the structure of the $[Mo_7O_{21}(O_3PCH_2PO_3)]^{4-}$ molecular anion of $[Ni_2(tpyprz)_2][M_7O_{21}(O_3PCH_2PO_3)]$ (**9**·$3.5H_2O$).

The polymeric cation $\{Ni(tpyprz)\}_n^{2n+}$ is structurally analogous to that observed for **10**. The observation of this cationic unit in both **9** and **10** suggested that catenation may be a common feature of the Ni(II)/tpyprz chemistry, a conclusion reinforced by subsequent structural investigations.

Variations in synthetic conditions produced a second nickel−molybdate material incorporating methylenediphosphonate subunits, $[\{Ni_2(tpyprz)(H_2O)_2\}(Mo_3O_8)_2(O_3PCH_2O_3)_2]$ (**1**), shown in Figure 3a. The structure is constructed from $\{(Mo_3O_8)_2(O_3PCH_2PO_3)_2\}_n^{4n-}$ chains, linked through $\{Ni_2(tpyprz)(H_2O)_2\}^{4+}$ complex binuclear cations into a three-dimensional framework. The molybdophosphonate chain is constructed from trinuclear clusters of edge-sharing $\{MoO_6\}$ octahedra linked through the methylenediphosphonate ligands. The central molybdenum of the triad shares cis-edges with

(52) Burkholder, E.; Golub, V. O.; O'Connor, C. J.; Zubieta, J. *Inorg. Chim. Acta* **2002**, *340*, 127.
(53) Barthelet, K.; Nogues, M.; Riou, D.; Ferey, G. *Chem. Mater*. **2002**, *14*, 4910.

Table 2. Summary of Structural Characteristics of the Oxomolybdate−Organophosphonate/Ni(II)−tpyprz Compounds of This Study and a Comparison to the Compounds of the Oxomolybdate−Organophosphonate/Cu(II)−tpyprz Series

compound (*n*, tether length)	overall dimension	M(II) (tpyprz) substructure and M(II) coordination mode	M(II)/molybdate substructure	phosphomolybdate substructure
$[\{Ni_2(tpyprz)(H_2O)_2\}(Mo_3O_8)_2(O_3PCH_2PO_3)_2]$ (**1**) ($n = 1$)	3-D	$\{Ni_2(tpyprz)(H_2O)_2\}^{4+}$ binuclear unit; $\{NiN_3O_3\}$.	pentanuclear cluster, $\{Ni_2Mo_3\}$	$\{(Mo_3O_8)_2(O_3PCH_2PO_3)_2\}_n^{4n-}$ chain
$[Ni_2(tpyprz)_2][Mo_7O_{21}(O_3PCH_2PO_3)]$ (**9**) ($n = 1$)	0 and 1-D	$\{Ni(tpyprz)\}_n^{2n+}$ chains; $\{NiN_6\}$	No Mo−O−Ni bonding	$[Mo_7O_{21}(O_3PCH_2PO_3)]^{4-}$ clusters
$[\{Cu_2(tpyprz)(H_2O)_2\}(Mo_3O_8)_2(O_3PCH_2PO_3)_2]$ (**2**) ($n = 1$)	3-D	$\{Cu_2([tpyprz)(H_2O)_2^{4+}$ binuclear unit; $\{CuN_3O_3\}$	pentanuclear cluster, $\{Cu_2Mo_3\}$	$\{(Mo_3O_8)_2(O_3PCH_2PO_3)_2\}^{4n-}$ chain
$[\{Cu_2(tpyprz)(H_2O)\}(Mo_3O_8(HO_3PCH_2PO_3)_2]$ ($n = 1$)	1-D	$\{Cu_2(tpyprz)(H_2O)\}^{4+}$ binuclear unit; $\{CuN_3O_2\}$ square pyramids	no Mo−O−Cu bonding	$\{(Mo_3O_8)(HO_3PCH_2PO_3)_2\}_n^{4n-}$ clusters
$[\{Cu_2(tpyprz)(H_2O)\}_2(Mo_3O_8)_2(O_3PCH_2PO_3)_3]$ ($n = 1$)	1-D	$\{Cu_2(tpyprz)(H_2O)\}^{4+}$ binuclear unit; $\{CuN_3O_2\}$ square pyramids	No Mo−O−Cu bonding	$\{(Mo_3O_8)_2(O_3PCH_2PO_3)_3\}^{8-}$ clusters
$[\{Ni_4(tpyprz)_3\}\{Mo_5O_{15}(O_3PCH_2CH_2PO_3)\}_2]$ (**3**) ($n = 2$)	2-D	$\{Ni_4(tpyprz)_3\}^{+8}$ tetranuclear unit; $\{NiN_6\}$ and $\{NiN_3O_3\}$	chains	$\{Mo_5O_{15}(O_3PCH_2CH_2PO_3)\}_n^{4n-}$ chains
$[\{Cu_2(tpyprz)(H_2O)_2\}Mo_5O_{15}(O_3PCH_2CH_2PO_3)]$ ($n = 2$)	2-D	$\{Cu_2(tpyprz)(H_2O)_2\}^{+4}$ binuclear unit; $\{CuN_3O_2\}$ square pyramid and $\{CuN_3O_3\}$ 4 + 2 octahedron	$\{Cu_4Mo_{10}\}$ cluster	$\{Mo_5O_{15}(O_3PCH_2CH_2PO_3\}_n^{4n-}$ chains
$[\{Ni_2(tpyprz)(H_2O)_3\}Mo_5O_{15}\{O_3P(CH_2)_3PO_3\}]$ (**4**) ($n = 3$)	3-D	$\{Ni_2(tpyprz)(H_2O)_3\}^{4+}$ binuclear units; $\{NiN_3O_3\}$	chains	$[Mo_5O_{15}\{O_3P(CH_2)_3PO_3\}]_n^{4n-}$ chains
$[\{Cu_2(tpyprz)(H_2O)_2\{Mo_5O_{15}\}O_3P(CH_2)_3PO_3\}]$ ($n = 3$)	3-D	$\{Cu_2(tpyprz)(H_2O)_2\}^{4+}$ binuclear units; $\{CuN_3O_3\}$ 4 + 2 octahedra	2-D network	$[Mo_5O_{15}\{O_3P(CH_2)_3PO_3\}]_n^{4n-}$ chains
$[\{Ni_3(tpyprz)_2(H_2O)_2\}(Mo_5O_{15})(Mo_2F_2O_4)\{O_3P(CH_2)_3PO_3\}_2]$ (**5**) ($n = 3$)	2-D	$\{Ni_3(tpyprz)_2(H_2O)_2\}^{6+}$ trinuclear units; $\{NiN_6\}$ and $\{NiN_3O_3\}$	$\{Ni_2Mo_5\}$ clusters	$[(Mo_5O_{15})(Mo_2O_4F_2)\{O_3P(CH_2)_3PO_3\}]_n^{6n-}$ chains
$[\{Ni_2(tpyprz)_2\{Mo_5O_{15}\}O_3P(CH_2)_4PO_3\}]$ (**6**) ($n = 4$)	1-D	$\{Ni_2(tpyprz)_2\}^{4+}$ binuclear units; $\{NiN_6\}$ and $\{NiN_3O_3\}$	chain	$[(Mo_5O_{15})\{O_3P(CH_2)_4PO_3\}]_n^{4n-}$ chains
$[\{Cu_2(tpyprz)(H_2O)_2\}Mo_5O_{15}\{O_3P(CH_2)_4PO_3\}]$ ($n = 4$)	3-D	$\{Cu_2(tpyprz)(H_2O)_2\}^{4+}$ binuclear units; $\{CuN_3O_3\}$ 4 + 2′ octahedra	2-D network	$[Mo_5O_{15}\{O_3P(CH_2)_4PO_3\}]_n^{4n-}$ chains
$[\{Ni_2(tpyprz)(H_2O)_2\}Mo_5O_{15}\{O_3P(CH_2)_4PO_3\}]$ (**7**) ($n = 4$)	3-D	$\{Ni(tpyprz)(H_2O)_2\}^{4+}$ binuclear units; $\{NiN_3O_3\}$	2-D network	$[Mo_5O_{15}\{O_3P(CH_2)_4PO_3\}]_n^{4n-}$ chains
$[\{Ni_2(tpyprz)_2\}Mo_5O_{15}\{O_3P(CH_2)_5PO_3\}]$ (**8**) ($n = 5$)	1-D	$\{Ni_2(tpyprz)_2\}^{4+}$ binuclear unit; $\{NiN_6\}$ and $\{NiN_3O_3\}$	chain	$[Mo_5O_{15}\{O_3P(CH_2)_5PO_3\}]_n^{4n-}$ chain
$[Ni_2(tpyprz)_2][Mo_6O_{18}(H_2O)(O_3PC_6H_5)_2]$ (**9**)	0 and 1-D	$\{Ni(tpyprz)\}_n^{2n+}$ chains; $\{NiN_6\}$	No Mo−O−Ni bonding	$[Mo_6O_{18}(H_2O)(O_3PC_6H_5)_2]^{4-}$ clusters
$[\{Cu_2(tpyprz)(H_2O)Mo_5O_{15}(O_3PC_6H_5)_2]$	1-D	$\{Cu_2(tpyprz))H_2O)\}^{4+}$ binuclear unit; $\{CuN_3O\}$ square planar and $\{CuN_3O_2\}$ square pyramid	$\{CuMo_5\}$ cluster	$[Mo_5O_{15}(O_3PC_6H_5)_2]^{4-}$ clusters

the exterior $\{MoO_6\}$ octahedra. Each molybdenum site exhibits two terminal oxo groups; the central Mo site participates in two doubly bridging oxo interactions and two $\{P-O-Mo_2\}$ bridges, while the exterior Mo centers each participate in one $\{Mo-O-Mo\}$ bridge, one $\{P-O-Mo_2\}$ bridging linkage, one phosphonate oxygen bond to the methylenediphosphonate of the $\{Mo_3O_8(O_3PCH_2PO_3)\}$ cluster, and a bond to a diphosphonate of a neighboring cluster. As a result of this connectivity pattern, each methylenediphosphonate ligand in turn directs four oxygen donors to the Mo triad of the cluster and employs one oxygen donor at each $\{-PO_3\}$ terminus to link the cluster to two adjacent clusters of the chain.

The Ni(II)−tpyprz substructure adopts the common $\{Ni_2(tpyprz)(H_2O)_n\}^{4+}$ ($n = 2$ for compound **1**) binuclear motif. Each Ni(II) site coordinates in a meridional fashion to one terminus of the tpyprz and completes its coordination sphere by linking to terminal oxo groups from two $\{Mo_3O_8(O_3PCH_2PO_3)\}_n^{4n-}$ chains and to an aqua ligand. Consequently, each $\{Ni_2(tpyprz)(H_2O)_2\}^{4+}$ subunit links four $\{Mo_3O_8(O_3PCH_2PO_3)\}_n^{4n-}$ chains, two from each of two adjacent $\{Ni_2(Mo_3O_8)(O_3PCH_2PO_3)\}$ layers (Figure 3b). The structure may then be described alternatively as neutral bimetallic phosphonate oxide layers $\{Ni_2(Mo_3O_4)(O_3PCH_2PO_3)\}$ linked through tpyprz ligands into a three-dimensional framework.

While the Cu(II)−tpyprz chemistry of the oxomolybdenum−methylenediphosphoric acid system had previously revealed two one-dimensional structures, $[\{Cu_2(tpyprz)(H_2O)\}Mo_3O_8(HO_3PCH_2PO_3)_2]$ and $[\{Cu_2(tpyprz)(H_2O)\}_2(Mo_3O_8)_2(O_3PCH_2PO_3)_3]$ (Table 2), we found that by appropriate manipulation of reaction conditions a third phase,

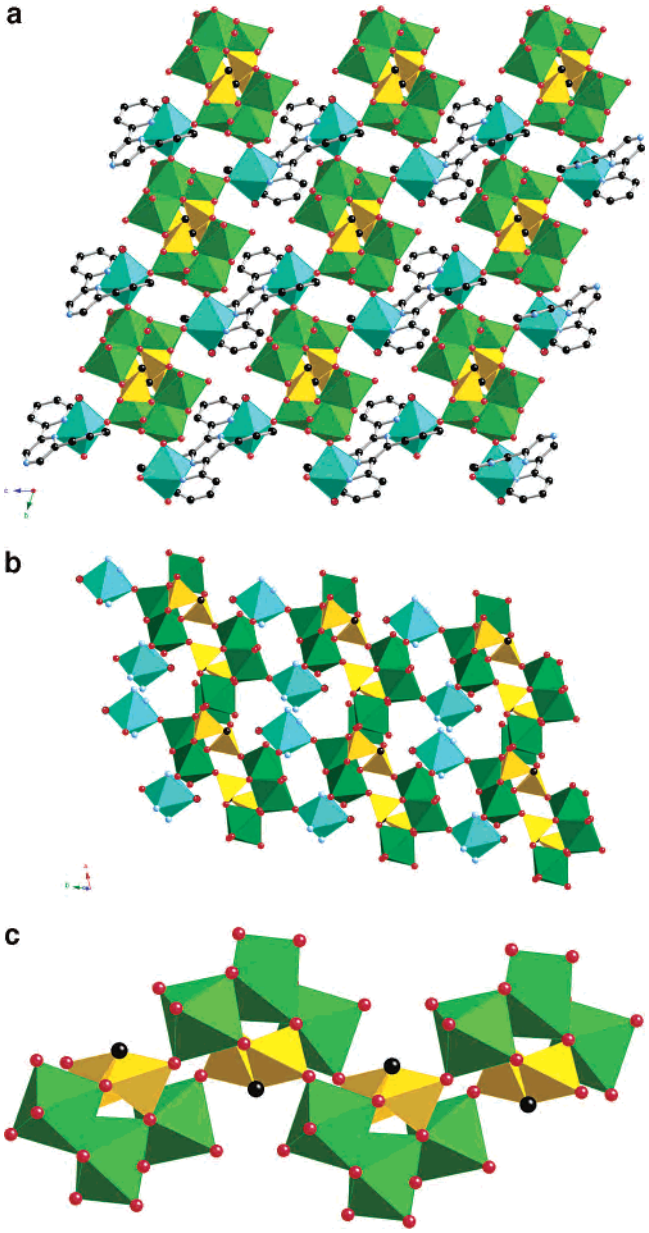

Figure 3. (a) Polyhedral representation of the three-dimensional structure of $[\{Ni_2(tpyprz)(H_2O)_2\}(Mo_3O_8)_2(O_3PCH_2PO_3)_2]$ (**1**), viewed normal to the *bc* plane. (b) The neutral bimetallic $\{NiMo_3O_8(O_3PCH_2PO_3)\}$ layer substructure of **1**. (c) The $\{Mo_3O_8(O_3PCH_2PO_3)\}_n^{2n-}$ chain of **1**.

Table 3. Secondary Metal Bond Lengths (Å) for $[\{M_2(tpyprz)(H_2O)_2\}(Mo_3O_8)_2(O_3PCH_2PO_3)_2]$ (M = Ni (**1**), Cu (**2**))

	1	**2**
$M-N_{pyrazine}$	2.001(2)	1.971(2)
$M-N_{pyridine}$	2.028(2)	1.983(2)
	2.044(2)	1.995(2)
$M-O_{aqua}$	2.081(2)	2.213(2)
$M-O_{oxo}$	1.985(2)	1.952(2)
	2.080(2)	2.424(2)

isomorphous to **1**, $[\{Cu_2(tpyprz)(H_2O)_2\}(Mo_3O_8)_2(O_3PCH_2PO_3)_2]$ (**2**) could be isolated. The structures of **1** and **2** only differ significantly in the bond lengths, as shown in Table 3. As expected from the usual trends, the Cu−N bond distances are significantly shorter than the corresponding Ni−N bond lengths. However, the Jahn−Teller distortion

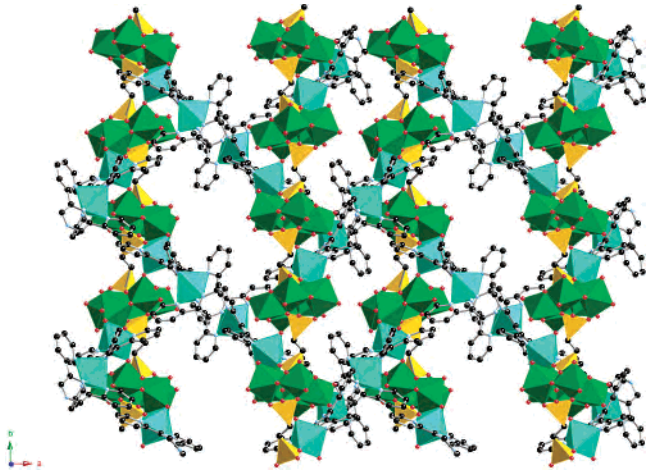

Figure 4. A polyhedral representation of the two-dimensional structure of $[\{Ni_4(tpyprz)_3\}Mo_5O_{15}\{(O_3PCH_2CH_2PO_3\})_2]\cdot 23H_2O$ (**3**·$23H_2O$) in the *ab* plane.

of the Cu(II)-d^9 geometry is observed as significant lengthening of the axial bonds to produce 4 + 2 geometry.

A significant feature of the structures of **1**, **2**, and the previously reported $[\{Cu_2(tpyprz)(H_2O)\}(Mo_3O_8)(HO_3PCH_2PO_3)_2]$ and $[\{Cu_2(tpyprz)(H_2O)\}_2(Mo_3O_8)_2\ (O_3PCH_2PO_3)_3]$ is the presence of the $\{Mo_3O_8(O_3PCH_2PO_3)\}^{n-}$ subunit. The Cu(II) structures exhibit an expansion of the oxomolybdophosphonate substructure from a trinuclear cluster $\{Mo_3O_8(HO_3PCH_2PO_3)_2\}^{4-}$ to a "dimer" of trinuclear clusters $\{(Mo_3O_8)_2(O_3PCH_2PO_3)_3\}^{8-}$ to a chain of clusters $\{Mo_3O_8(O_3PCH_2PO_3)\}_n^{2n-}$ in **2**, shown in Figure 3c. The structural determinant for the previously reported structures appears to be the Cu(II)/tpyprz stoichiometry, while the denser phase structure of **2** may be the consequence of higher temperature. This characteristic of the hydrothermal domain has been discussed in recent publications.[54]

Increasing the diphosphonate tether length results in the two-dimensional structure of $[\{Ni_4(tpyprz)_3\}\{Mo_5O_{15}(O_5PCH_2CH_2PO_3)\}_2]$ (**3**). As shown in Figure 4, the structure of **3** may be described as $\{Mo_5O_{15}(O_3PCH_2CH_2PO_3)\}_n^{4n-}$ chains linked through linear tetranuclear subunits $\{Ni_4(tpyprz)_3\}^{8+}$ into a network. The molybdophosphonate substructure is constructed from the common pentanuclear $\{Mo_5O_{15}(O_3PR)_2\}^{4-}$ clusters linked through the ethylene bridges of the diphosphonate ligand. The most unusual feature of the structure, as previously described, is the incorporation of the $\{Ni_4(tpyprz)_3\}^{8+}$ subunit which displays two unique Ni(II) sites: the terminal metal centers display $\{NiO_3N_3\}$ geometry through coordination to three nitrogen donors of the tpyprz ligand, two terminal oxo groups of two adjacent clusters of the molybdophosphonate chain, and a phosphonate {P−O−Mo} oxygen atom; the interior Ni(II) centers exhibit $\{NiN_6\}$ coordination through bonding to three nitrogen donors from each of two tpyprz ligands.

The structure of the corresponding Cu(II) material, $[\{Cu_2(tpyprz)(H_2O)_2\}Mo_5O_{15}(O_3PCH_2CH_2PO_3)]$, is constructed from an identical $\{Mo_5O_{15}(O_3PCH_2CH_2PO_3)\}_n^{4n-}$ chain to

(54) Forster, P. M.; Burbank, A. R.; Livage, C.; Ferey, G.; Cheetham, A. K. *Chem. Commun.* **2004**, 368.

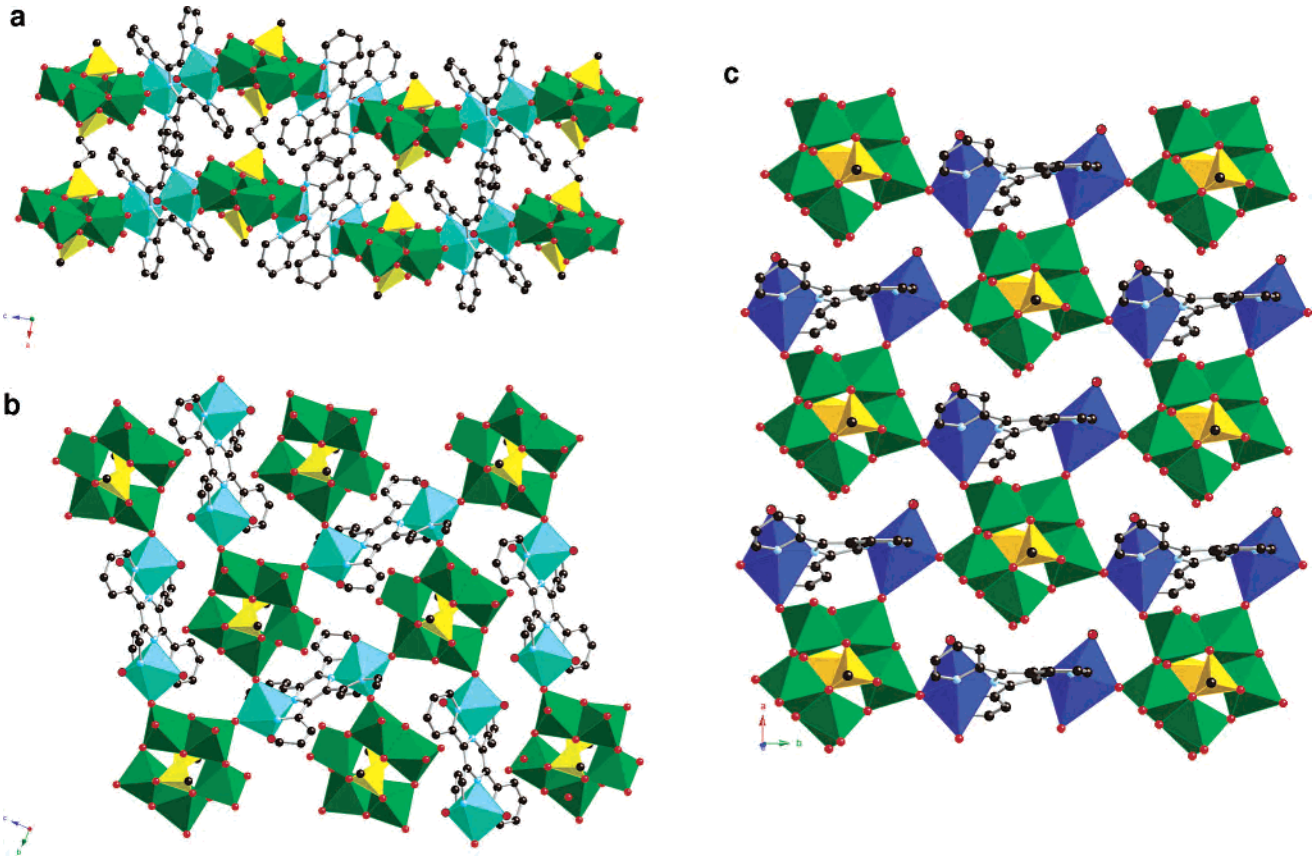

Figure 5. (a) A view of the three-dimensional structure of $[\{Ni_2(tpyprz)(H_2O)_3\}Mo_5O_{15}\ \{O_3P(CH_2)_3PO_3\}]\cdot H_2O$ (**4**·H_2O) parallel to the *b* crystallographic axis. (b) The $[\{Ni_2(tpyprz)(H_2O)_2\}\{Mo_5O_{15}(O_3PR)_2\}]_n$ neutral bimetallic network of **4** in the *bc* plane. (c) The corresponding $[\{Cu_2(tpyprz)(H_2O)_2\}Mo_5O_{15}(O_3PR)_2]_n$ layer of $[\{Cu_2(tpyprz)(H_2O)_2\{Mo_5O_{15}\}O_3P(CH_2)_3PO_3\}]$ in the *ac* plane.

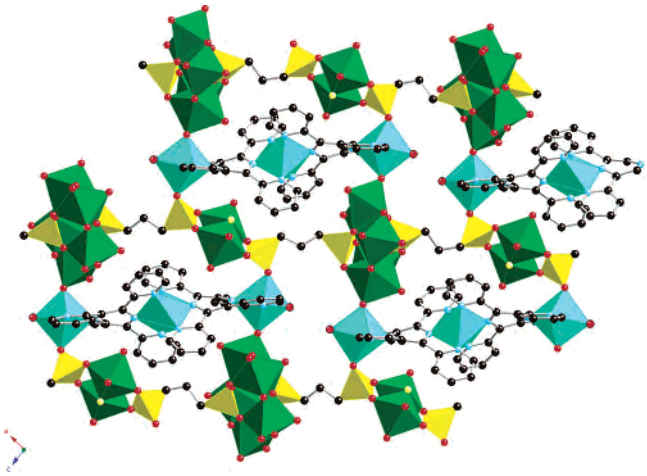

Figure 6. Polyhedral representation of the two-dimensional structure of $[\{Ni_3(tpyprz)_2(H_2O)_2\}(Mo_5O_{15})(Mo_2F_2O_4)\{O_3P(CH_2)_3PO_3\}_2]\cdot 8H_2O$ (**5**·$8H_2O$) in the *ac* plane.

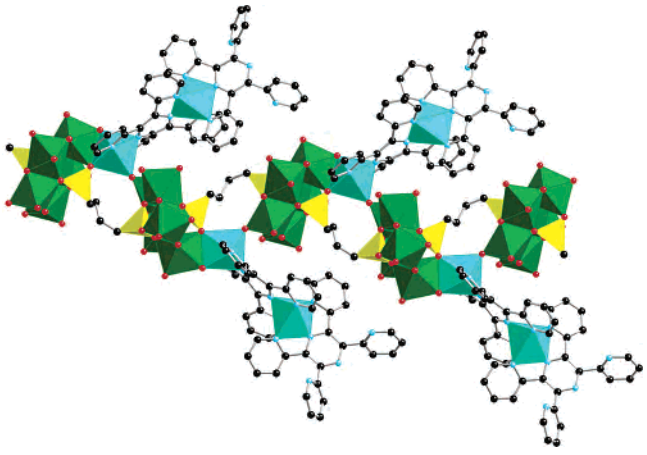

Figure 7. A view of the one-dimensional structure of $[\{Ni_2(tpyprz)_2\}Mo_5O_{15}\{O_3\ P(CH_2)_4PO_3\}]\cdot 6.65H_2O$ (**6**·$6.65H_2O$).

that of **3**. However, the chains are linked into a network structure through the conventional $\{Cu_2(tpyprz)(H_2O)_n\}^{4+}$ subunit. The incorporation of the extended tetranuclear chain in **3** results in an expansion of intralamellar cavities in **3**, compared to those of the Cu(II) material, which accommodate a significant amount of water of crystallization (ca. 23 H_2O per cavity).

Further extension of the diphosphonate tether reveals the three-dimensional materials $[\{Ni_2(tpyprz)(H_2O)_3\}Mo_5O_{15}\{O_3P(CH_2)_3PO_3\}]\cdot H_2O$ (**4**·H_2O) and $[\{Ni_2(tpyprz)(H_2O)_2\}Mo_5O_{15}\ \{O_3P(CH_2)_4PO_3\}]\cdot 2.25H_2O$ (**7**·$2.25H_2O$). Both structures contain the $\{Mo_5O_{15}(O_3PR)_2\}^{4-}$ cluster building block in the form of $\{Mo_5O_{15}O_3P(CH_2)PO_3\}_n^{4n-}$ chains, in common with the structure of **3**.

As shown in Figure 5a, the structure of **4** may be described as bimetallic nickel molybdophosphonate layers linked through the propylene tethers of the diphosphonate ligand into an overall three-dimensional covalent connectivity. A curious feature of the layer structure is the presence of two

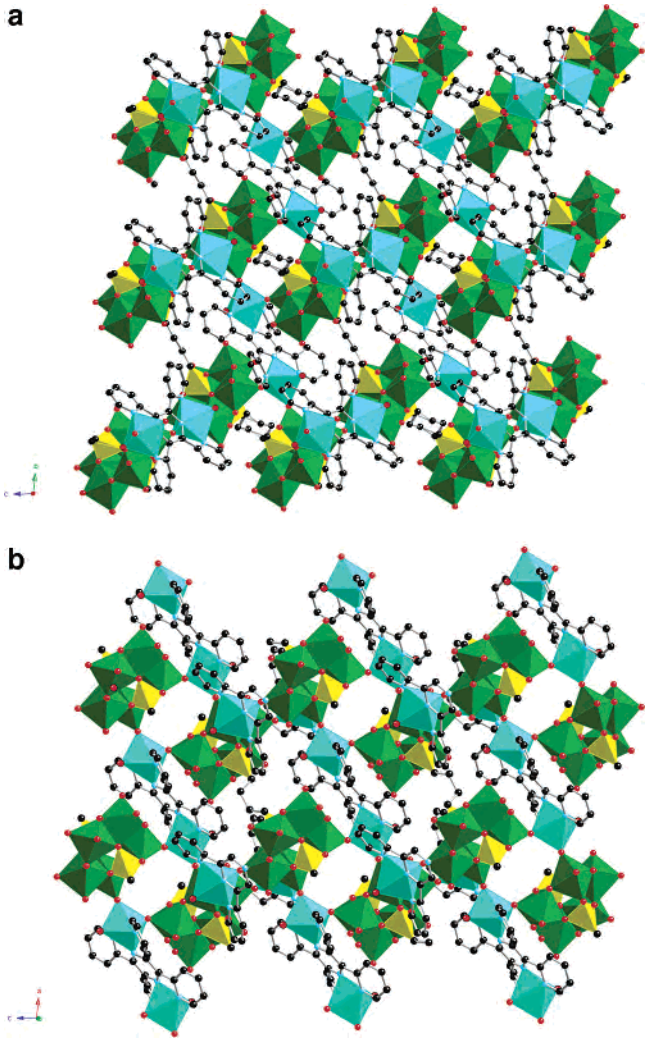

Figure 8. (a) Polyhedral representation of structure of $[\{Ni_2(tpyprz)(H_2O)_2\}Mo_5O_{15}\{O_3P(CH_2)_4PO_3\}]\cdot 2.25H_2O$ (**7**·2.25H_2O) normal to the *bc* plane. (b) The ruffled $[Ni_2Mo_5O_{15}\{O_3P(CH_2)_4PO_3\}]_n$ layer of **7** in the *ac* plane.

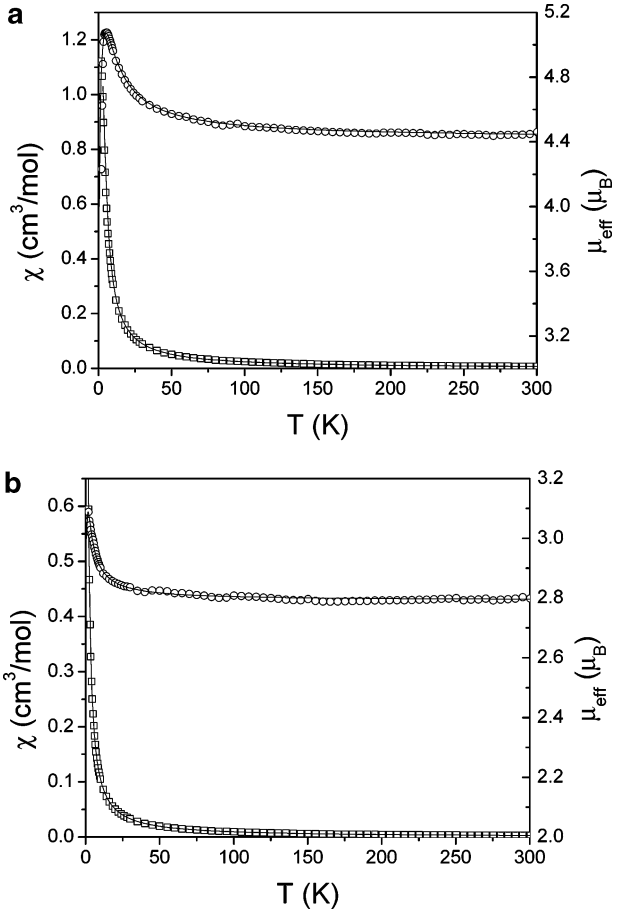

Figure 9. The dependence of the magnetic susceptibilities χ and effective magnetic moments μ_{eff} of **1** and **2** (a and b, respectively) on temperature *T*. The line drawn through the data is the fit to the Heisenberg dimer model.

discrete $\{Ni_2(tpyprz)(H_2O)_n\}^{4+}$ cationic subunits with n = 2 and 4. The building block $\{Ni_2(tpyprz)(H_2O)_2\}^{4+}$ completes the six coordination on the metal site through coordination to two oxo groups {Mo═O} from two molybdophosphonate chains to each Ni site in addition to the three nitrogen donors from the tpyprz and the aqua ligand. The aqua ligands are disposed in the anti orientation with respect to the $\{Ni_2(tpyprz)\}$ plane, allowing the binuclear subunit to link to four neighboring molybdophosphonate chains. The second Ni cluster $\{Ni_2(tpyprz)(H_2O)_4\}^{4+}$ displays two trans disposed aqua ligands on each Ni site, consequently leaving only a single site on each metal for bonding to the molybdophosphonate substructure (Figure 5b).

While the corresponding Cu(II) material $[\{Cu_2(tpyprz)(H_2O)_2\}Mo_5O_{15}\{O_3P(CH_2)_3PO_3\}]$ is also three-dimensional, the details of the connectivity within the layer are quite distinct, as illustrated in Figure 5c. In this case, there is a single $\{Cu_2(tpyprz)(H_2O)_2\}^{4+}$ subunit, which displays syn oriented aqua ligands. Each cationic building block links three adjacent molybdophosphonate chains, and each chain is linked to six adjacent chains (four proximal and two distal) through three $\{Cu_2(tpyprz)(H_2O)_2\}^{4+}$ units. In the copper structure, each molybdate cluster enjoys four points of contact with the three copper subunits through terminal oxo groups {Mo═O}. In contrast, in the structure of **4**, each cluster exhibits only three {Mo−O−Ni} interactions, one with each of three Ni(II)−tpyprz subunits. However, the connectivity pattern is such that each molybdophosphonate chain is linked through the two distinct Ni(II)−tpyprz subunits to six neighboring chains, four proximal and two distal, but in a tessellation pattern quite distinct from that of the corresponding Cu(II) material.

A second phase is isolated when propylenediphosphonic acid is used as the phosphonate component. The structure of $[\{Ni_3(tpyprz)_2(H_2O)_2\}(Mo_5O_{15})(Mo_2F_2O_4)\{O_3P(CH_2)_3PO_3\}_2]\cdot 8H_2O$ (**5**·8H_2O), as shown in Figure 6, is quite remarkable. Although the anticipated $\{Mo_5O_{15}(O_3PR)_2\}^{4-}$ building block is observed in the two-dimensional structure of **5**, a second molybdate cluster subunit is also incorporated, $\{Mo_2F_2O_4(O_3PR)_2\}^{2-}$. The structure may be described as chains constructed of alternating $\{Mo_5O_{15}(O_3PR_2\}^{4-}$ clusters and $\{Mo_2F_2O_4(O_3PR)_2\}^{2-}$ units linked through the propylene chains of the diphosphonate ligand. The molybdophosphonate chains are linked through trinuclear rods $\{Ni_3(tpyprz)_2(H_2O)_2\}^{6+}$ into the network structure.

The unusual binuclear molybdate component consists of two $\{MoF_2O_4\}$ octahedra sharing an edge defined by two

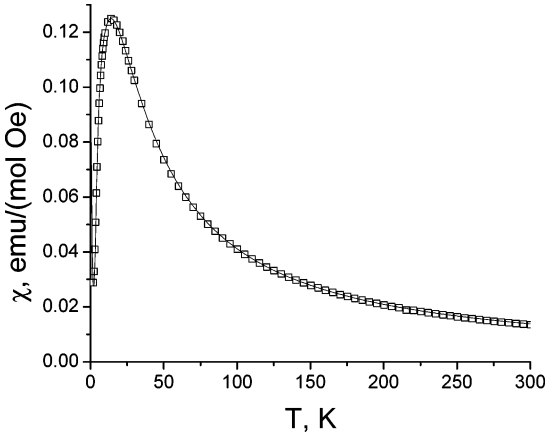

Figure 10. The dependence of the magnetic susceptibility χ of **3** with temperature *T*. The line drawn through the data is the fit to the Heisenberg linear tetramer model.

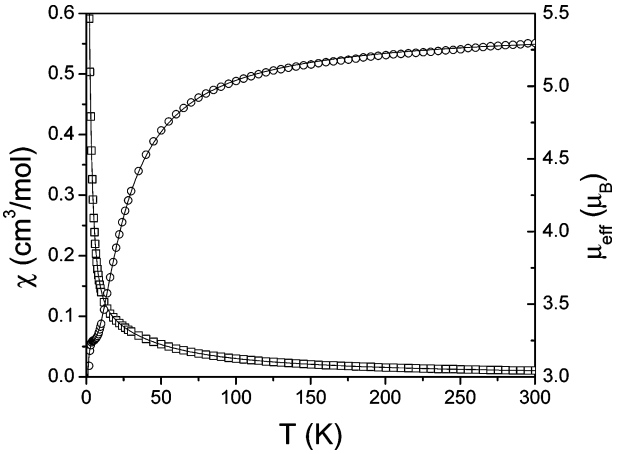

Figure 11. A plot of the dependence of the magnetic susceptibility and effect magnetic moment μ_{eff} of **5** on temperature *T*. The line drawn through the data is the fit to the Heisenberg linear trimer model.

bridging fluoride ligands with the remaining coordination at each Mo site consisting of cis-terminal oxo groups and two oxygen donors from propylenediphosphonate tethers of the chain. Such incorporation of fluoride into oxometalate structures is not unusual, and the $\{Mo_2F_2O_4(O_3PR)_2\}^{2-}$ unit of this study is reminiscent of the $\{Mo_2F_2O_4(MoO_4)_2\}^{2-}$ core previously described for the molecular compound $[Ni(tpyprz)_2]_2[Mo_4O_{12}F_2][Mo_6O_{19}]$.[50]

Catenation of the Ni(II)−tpyprz subunit is once again observed, in this case in the form of a trinuclear subunit $\{Ni_3(tpyprz)_2\}^{6+}$. The central Ni site exhibits $\{NiN_6\}$ geometry in bonding to the tridentate termini of two tpyprz ligands; the $\{NiN_3O_3\}$ coordination of the peripheral Ni sites is defined by the remaining three nitrogen donors of the tpyprz ligand, an oxo group (Mo═O) of a molybdophosphonate chain, a phosphate oxygen donor (P−O−Ni) of an adjacent chain, and an aqua ligand. Curiously, the cationic rods do not radiate outward from the molybdophosphonate chain but rather orient parallel to these chains.

One consequence of this unusual juxtaposition of structural elements is the creation of interlamellar cavities of dimensions 4.3 Å × 8.8 Å, enclosed within a ring of 10 polyhedra

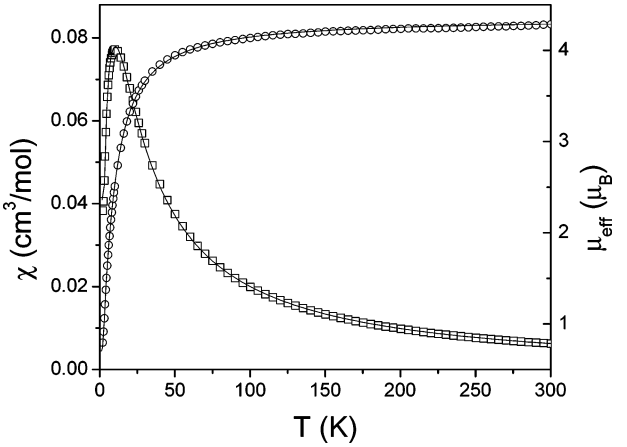

Figure 12. Plot of the dependence of the magnetic susceptibility χ and effective magnetic moment of **7** on temperature *T*. The inset shows the dependence of $1/\chi$ with temperature *T*. The line through the data is the fit to the Heisenberg dimer model.

(22-membered heterocycle). The aqua ligands from two adjacent $\{Ni_3(tpyprz)_2\}^{6+}$ units project into each of these cavities.

With butylenediphosphonate, two materials are isolated under slightly modified conditions, the one-dimensional $[\{Ni_2(tpyprz)_2\}Mo_5O_{15}\{O_3P(CH_2)_4PO_3\}]\cdot 6.65H_2O$ (**6**·6.65H_2O) and the three-dimensional $[\{Ni_2(tpyprz)(H_2O)_2\}Mo_5O_{15}\{O_3P(CH_2)_4PO_3\}]\cdot 2.25H_2O$ (**7**·2.25H_2O). The structure of the one-dimensional material is in general unexceptional. As shown in Figure 7, the structure of **6** is constructed from the nearly ubiquitous $\{Mo_5O_{15}(O_3PR)_2\}^{4-}$ clusters linked through the butylene tethers of the diphosphonate. However, these molybdophosphonate chains are not cross-linked by the Ni(II) subunit as one of the Ni sites has its coordination satisfied by a second tpyprz ligand. Thus, one Ni exhibits $\{NiN_3O_3\}$ geometry but in a rather unusual fashion by bridging Mo centers of two adjacent clusters within a single chain. Thus, this nickel coordinates to the three nitrogen donors of the tpyprz ligand, shares a corner with one Mo site through a terminal {Mo═O} group, and shares an edge with the second Mo site through a terminal oxo group and a bridging phosphonate oxygen {Mo−O(P)−Ni}. The second Ni site exhibits $\{NiN_6\}$ coordination, and the terminal tpyprz ligand projects two pendant pyridyl groups into the interchain domain.

The pentyldiphosphonate compound $[\{Ni_2(tpyprz)_2\}Mo_5O_{15}\{O_3P(CH_2)_5PO_3\}]\cdot 3.75H_2O$ (**8**·3.75H_2O) is isomorphous with **6**. The only significant structural difference is the lengthening of the distance between molybdophosphonate clusters as a consequence of the extension of the tether length (6.1 Å in **6** vs 6.6 Å for **8**).

By adjusting the Ni:tpyprz ratio for the butyldiphosphonate containing subgroup, the three-dimensional material **7**·2.25H_2O, shown in Figure 8a, was isolated. While the structure of **7** is constructed from the common building blocks $\{Mo_5O_{15}(O_5PR)_2\}^{4-}$ clusters and $\{M_2(tpyprz)(H_2O)_n\}^{4+}$ as was the case for **4**, the juxtapositioning of structural elements is quite distinct. The structure may be described as bimetallic nickel molybdophosphonate sheets

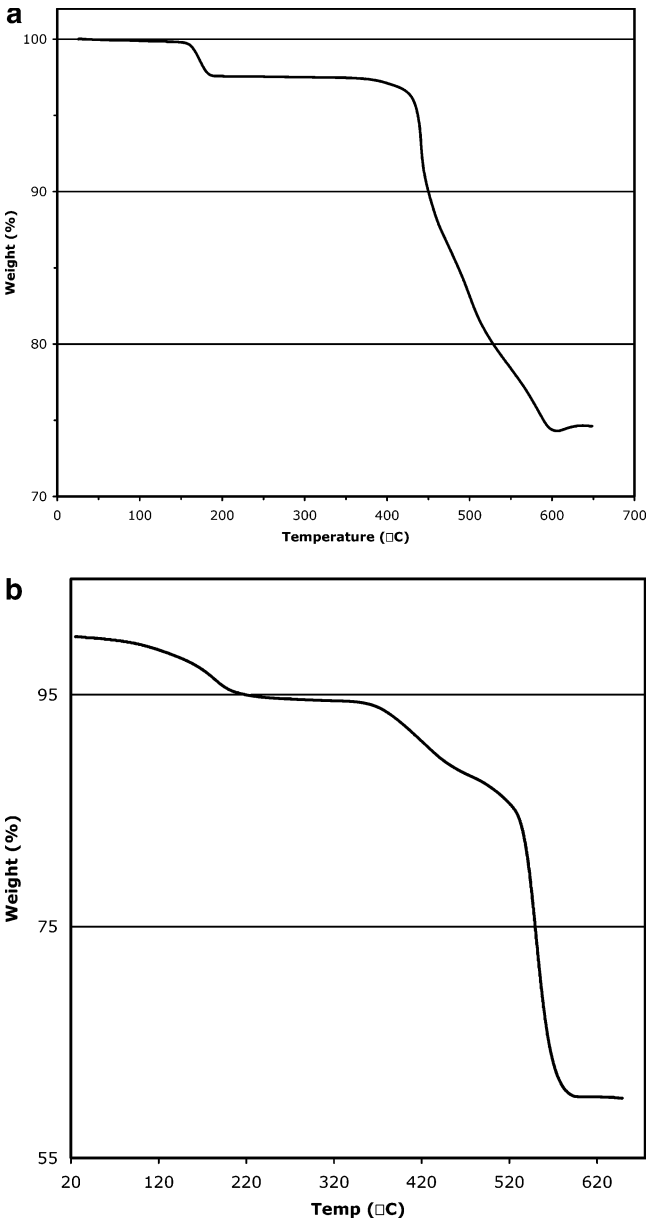

Figure 13. Thermal gravimetric analysis (TGA) curves for (a) $[\{Cu_2(tpyprz)(H_2O)_2\}(Mo_3O_8)_2(O_3PCH_2PO_3)_2]$ (**2**) and (b) $[\{Ni_3(tpyprz)_2(H_2O)_2\}(Mo_5O_{15})(Mo_2F_2O_4)\{O_3P(CH_2)_3PO_3\}_2]\cdot 8H_2O$ (**5**·$8H_2O$).

linked through $\{Ni_2(tpyprz)(H_2O)_2\}^{4+}$ rods into the overall three-dimensional connectivity. The $[Mo_5O_{15}\{O_3P(CH_2)_4PO_3\}]_n^{4n-}$ chains run parallel to the *bc* plane and are linked in this plane by $\{Ni(tpyprz)(H_2O)_2\}^{4+}$ rods which orient parallel to the molybdophosphonate chains. Each chain is associated with two of the Ni rods and linked to two adjacent chains in the layer. The second type of $\{Ni_2(tpyprz)(H_2O)_2\}^{4+}$ rod projects above and below this $[Ni_2(tpyprz)(H_2O)_2Mo_5O_{15}\{O_3P(CH_2)_4PO_3\}]_n^{4n-}$ plane and serves to link each plane to two adjacent planes in establishing the three-dimensional connectivity.

It is noteworthy that while the copper structures $[\{Cu_2(tpyprz)(H_2O)_2\}Mo_5O_{15}\{O_3P(CH_2)_nPO_3\}]$ ($n = 3$ and 4) are isostructural, the corresponding nickel structures **4** and **7** are not. In the structure of **4**, the Ni(II)−tpyprz rods are exclusively involved in the connectivity within the $[Ni_2(tpyprz)(H_2O)_2Mo_5O_{15}(O_3PR)_2]$ bimetallic neutral layer, and three-dimensional connectivity is achieved through the propylene bridges. In contrast, the structure of **7** displays two distinct Ni(II)−tpyprz structural units, one orienting parallel to the diphosphonate tethers and the second adopting a nearly perpendicular orientation.

The corresponding three-dimensional material could not be isolated for the pentyldiphosphonate subgroup, despite repeated attempts. While this observation may simply imply that the appropriate conditions for synthesis remain elusive, the charge density matching between constituent building blocks may not be suitable for construction of the three-dimensional framework analogous to **7**.

Magnetism. Since the molybdenum(VI)−organophosphonate substructures of the solid phases **1** and **3**−**8** are diamagnetic, the paramagnetism of the materials resides in the d^8-Ni(II) sites. However, the range of Ni−tpyprz substructures displayed by these phases produces a range of magnetic properties, reflecting the weak antiferromagnetic interactions between the Ni(II) sites.

The dependence of magnetic susceptibility χ and effective magnetic moment μ_{eff} on temperature for **1** and **2** is shown in Figure 9. The effective moments ($\mu_{eff} = (8(\chi - \chi_{TI})T)^{1/2}$, where χ_{TI} is a temperature independent contribution to the magnetic susceptibility and includes temperature independent paramagnetism, TIP, and the diamagnetic contribution) of both compounds increases with decreasing temperature, indicating the presence of intramolecular ferromagnetic interactions within the $\{M_2(tpyprz)\}^{4+}$ subunits. The decrease in the moment of **2** below 5 K indicates that there is a weak antiferromagnetic interaction between binuclear sites. The best description of the experimental results for the Cu(II) material **2** is provided by the Heisenberg dimer model with $S = {}^1/_2$

$$\chi = \frac{N_A g^2 \mu^2_B}{k_B T} \frac{2e^{2x}}{1 + 3e^{2x}} + \chi_{TI}$$

The best fit gave $g = 2.28$, $J/k_B = 2.0$ K, $\chi_{TI} = -0.00035$ cm^3/mol. The effective magnetic moment at 300 K is 2.80 μ_B/binuclear site. For the Ni(II) material **1**, the Heisenberg dimer model with $S = 1$ was employed.

$$\chi = \frac{N_A g^2 \mu_B^2}{k_B T} \frac{2e^{2x} + 10^{6x}}{1 + 3e^{2x} + 7e^{6x}} + \chi_{TI}$$

where $x = J/k_BT$. The calculated susceptibility χ has been corrected for the exchange interaction zJ′ between$\{Ni_2(tpyprz)\}^{4+}$ sites.

$$\chi' = \frac{\chi}{1 - (2zJ'/Ng^2\mu_B^2)\chi}$$

The best fit was $g = 2.21$, $J/k_B = 3.1$ K, $zJ'/k_B = -0.13$, $\chi_{TI} = 0.0001$ cm^3/mol. The effective magnetic moment at 300 K is 4.45 μ_B per $\{Ni_2(tpyprz)\}^{4+}$ binuclear site.

The dependence of magnetic susceptibility on temperature for **3** is illustrated in Figure 10. The maximum susceptibility at ca. 14 K indicates the presence of antifer-

romagnetic interactions between Ni(II) sites. The results were modeled using the Heisenberg tetramer model ($S = 1$) with the Hamiltonian

$$H = -2J(S_1S_2 + S_2S_3 + S_3S_4) - g\mu_B H\sum_{i=1}^{4} S_i$$

The calculated susceptibility χ has been corrected for intratetranuclear unit exchange interactions, zJ.

$$\chi' = \frac{\chi}{1 - (2zJ/Ng^2{\mu_B}^2)\chi}$$

The best fit gave $g = 2.10$, $J = -7.0$ K, $zJ = 2.3$ K, $TI = 0.00073$. While the Heisenberg tetramer model provides a possible explanation for the magnetic properties of this material, the data for **3** and other members of this family may reflect the single-ion magnetic anisotropy of Ni(II). However, we were unable to extract zero-field splittings from measurements of the low-temperature magnetization as a function of field.

The magnetic data for compound **5** are shown in Figure 11. The decrease of the effective moment with decreasing temperature is consistent with the presence of intracluster antiferromagnetic interactions within the $\{Ni_3(tpyprz)_2\}^{6+}$ subunit. At low temperature, there is a saturation of the magnetic moment at ca. 3.2 μ_B, which is characteristic of an antiferromagnetically coupled trimer with $S = 1$ at each site. The continued decrease of the moment with decreasing temperature beyond this point suggests intertrimer antiferromagnetic exchange. The best description of the experimental results is provided by the Heisenberg linear trimer model for $S = 1$.

$$\chi = \frac{N_A g^2 {\mu_B}^2}{k_B T}\frac{28e^{10x} + 10e^{8x} + 2e^{6x} + 12e^{4x} + 2}{7e^{10x} + 5e^{8x} + 3e^{6x} + 8e^{4x} + e^{8x} + 3}$$

where $x = J/k_BT$. The calculated susceptibility χ has been corrected for interdimer exchange interactions zJ'

$$\chi' = \frac{\chi}{1 - (2zJ'/Ng^2{\mu_B}^2)\chi}$$

The best fit gave $g = 2.21$, $J/k_B = -7.9$ K, $\chi_{TI} = -0.0015$ cm^3/mol. The effective magnetic moment at 300 K is 5.29 μ_B per trimer, corresponding to 3.05 μ_B per Ni(II) center.

The magnetic behavior of **6** reveals the presence of intraunit antiferromagnetic interactions within the $\{Ni_2(tpyprz)_2\}^{4+}$ binuclear subunit of the structure. The Heisenberg dimer model for $S = 1$ gave $g = 2.18$, $J/k_B = -5.6$ K, $zJ' = -1.0$, $\chi_{TI} = -0.0014$ cm^3/mol. The effective magnetic moment at 300 K is 4.29 μ_B per dimer, corresponding to 3.03 μ_B per Ni(II) site.

The dependence of the magnetic susceptibility and the effective magnetic moment on temperature for **7** is shown in Figure 12. The results may be adequately described by the Heisenberg dimer model ($S = 1$) which gave $g = 2.28$, $J/k_B = -0.95$ K, $\chi_{TI} = -0.0011$ cm^3/mol. The effective magnetic moment at 300 K is 4.55 μ_B (3.22 μ_B per NI(II) site).

Thermal Analyses. The thermogravimetric profiles of **2** and **5**·8H_2O are shown in Figure 13, parts a and b, respectively. In the case of **2** which contains only Cu-bound water, there is no weight change up to ca. 170 °C, whereupon there is a weight loss of 2.3%, corresponding to the loss of two water molecules (2.1%, calcd). This weight loss is followed by a plateau of stability from 190 to 380° C,

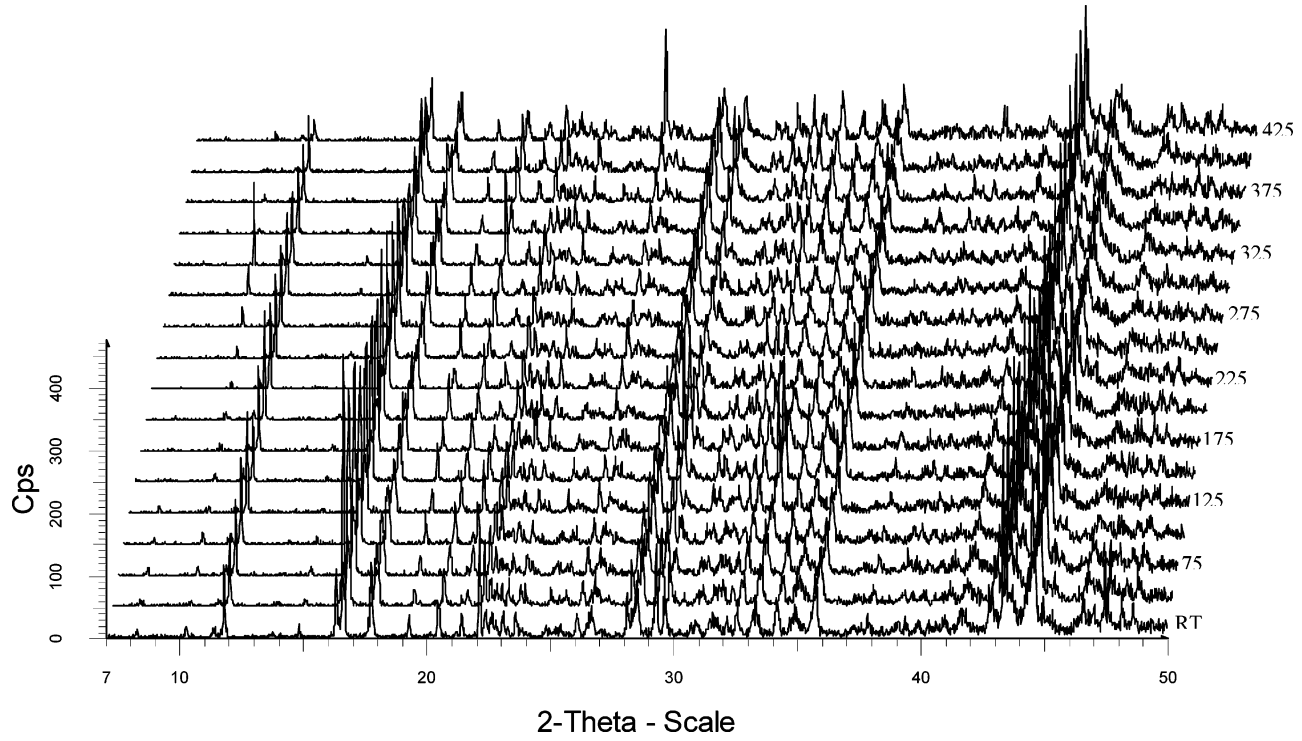

Figure 14. Thermodiffraction pattern for compound **1** in the 30−425 °C temperature range. Compound **2** provides a similar diffraction pattern.

whereupon there is a gradual weight loss of 36.2% from 380 to 600 °C, corresponding to the loss of the tpyprz ligand and the tether of the diphosphonate group (24.1%, calcd). The increase is weight above this temperature results from the uptake of oxygen to form pyrophosphate. Compound **1** exhibits nearly identical thermal properties.

In contrast to **1** and **2**, the TGA of **5**·8H_2O exhibits water loss immediately on heating, indicative of facile accessibility of the channels within the structure to water molecules of crystallization,[55] an observation consistent with the structure described previously. The water is lost gradually from room temperature to 185 °C with a weight loss of 5.5% (5.8%, calcd). The tpyprz ligand and the organic tether of the diphosphonate are released between 340 and 610 °C, a weight loss of 36.2% (35.7%, calcd).

In the case of compound **7**·2.25H_2O, water is lost in two steps. The first weight loss of 2.6% (2.7%, calcd) between room temperature and ca. 200 °C corresponds to the removal of the loosely held water of crystallization, while a second step from 210 to 350 °C corresponds to the loss of the aqua ligands. (2.4%, obsd; 2.4%, calcd). The tpyprz ligand and the organic tether are burned off in the range 350−600 °C with a weight loss of 29.7% (29.2%, calcd).

Thermodiffraction. The thermodiffraction pattern for compound **1** in the temperature range 25−425 °C is shown in Figure 14. The X-ray profile of **1** persists to ca. 300 °C, whereupon some minor changes are observed. Since the aqua ligands of crystallization are lost in the 170−200 °C range, this observation confirms that dehydration does not collapse the framework of **1** whose structure is retained well beyond the dehydration temperature. While some changes in the diffraction pattern begin to appear above 300 °C, the structure does not collapse until temperatures above 400 °C are attained, which correlates with the decomposition of the organic components of the structure. On cooling, the resultant poorly crystalline phase persists to room temperature. Heating above 450 °C results in a mixture predominantly composed of $NiMoO_4$, γ-MoO_3, and $Ni_2P_2O_7$.

Conclusions

Hydrothermal methods have been shown effective in the isolation of a new family of hybrid materials constructed from oxomolybdophosphonate anionic components and secondary metal−organic cations. The structures of compounds **1**−**8** reveal the persistence of two oxomolybdophosphonate building blocks. In the case of methylenediphosphonate as the tetrahedral building block, the short tether length does not permit extension of the molybdophosphonate substructure through the phosphate termini of this ligand, preventing the formation of the common $\{Mo_5O_{15}(O_3PR)_2\}^{4-}$ building block. However, the methylenediphosphonate chemistry of both the Cu(II) and Ni(II) families of materials reveals another common building block, the trinuclear $\{Mo_3O_8(O_3PCH_2PO_3)\}^{2-}$ cluster, which appears as a single unit, as a dimer of clusters, and as a chain of clusters in the various structures of the oxomolybdomethylenediphosphonate/M(II)−tpyprz family.

The $\{Mo_5O_{15}(O_3PR)_2\}^{4-}$ substructure is nearly ubiquitous in this structural chemistry and appears as a component of structures **3**−**8**. While both the Cu(II) and Ni(II) families of materials share this structural motif, the details of the connectivities between building blocks are often quite distinct (Table 2). In fact, a comparison of the structural systematics of the Ni(II) materials and their corresponding Cu(II) species reveals the importance of the identity of the secondary metal cation as a structural determinant. Certainly, one would anticipate that the coordination requirements of the secondary metal would be reflected in the structures of these materials, a point dramatically illustrated in contrasting the Cu(II) and Ni(II) structures.

While Cu(II) displays Jahn−Teller distorted geometries (square planar, 4 + 1, and 4 + 2 distorted six coordination), Ni(II) exhibits much more regular octahedral coordination. Consequently, while Cu(II) will bind exclusively to a single terminus of the tpyprz ligand to form the $\{Cu_2(tpyprz)\}^{4+}$ subunit with $\{CuN_3O\}$, $\{CuN_3O_2\}$, or $\{CuN_3O_3\}$ coordination modes adopted upon linking to the oxide substructure through one, two, or three attachment points, Ni(II) can achieve regular octahedral geometry by coordination to two tpyprz ligands to give $\{NiN_6\}$ coordination geometry. The balance between this tendency to assume regular octahedral geometry and the oxophilicity of Ni(II) results in varying degrees of oligomerization, resulting in $\{Ni_2(tpyprz)(H_2O)_n\}^{4+}$, $\{Ni_3(tpyprz)_3\}^{6+}$, $\{Ni_4(tpyprz)_3\}^{8+}$, and $\{Ni(tpyprz)\}_n^{2n+}$ coordination cations. Consequently, the structural chemistry of the Ni(II) family is considerably expanded in comparison to the Cu(II) family by virtue of such oligomerization. Furthermore, while the $\{Cu_2(tpyprz)\}^{4+}$ subunit may adopt one, two, or three points of attachment to the oxide component, the Ni(II) containing materials uniformly attach through three points of the $\{NiN_3O_3\}$ coordination mode as a consequence of this strong preference for six coordination. These significant differences in the coordination preferences of Cu(II) and Ni(II) are reflected in the structural systematics.

It is noteworthy, however, that structural isomorphism is encountered in the corresponding members of the Cu(II) and Ni(II) families, as noted for compounds **1** and **2**. In contrast, as we proceed along the series of increasing diphosphonate tether lengths, we note that while the materials may exhibit identical stoichiometries and overall dimensionalities, as for $[\{M_2(tpyprz)(H_2O)\}Mo_5O_{15}\{O_3P(CH_2)_4PO_3\}]$, the detailed connectivity patterns are quite distinct.

It is now established that under reaction conditions favoring the self-assembly of $\{Mo_5O_{15}(O_3PR)_2\}^{4-}$ clusters that a molecular building block approach to oxide materials is feasible. However, total predictability of structure remains elusive due to the complexity of hydrothermal parameter space and the diversity of linkage modes available to the constituent building blocks. The structural determinants include pH and temperature. A pH in the range of 1.5−2.5 is required for cluster formation via condensation to provide the pentamolybdate building blocks. The temperature domain has been shown to be important, as different structure types may be isolated by raising or lowering the reaction temper-

ature. In addition to the identity of the secondary metal and its ancillary ligand, the number of aqua ligands associated with a secondary metal complex determines the number of coordination sites available for linkage to the oxide components. Furthermore, the secondary metal may link to terminal or bridging oxo groups of the molybdate substructure or to phosphonate oxygen donors, as well as participating in corner- or edge-sharing interactions with the molybdenum sites. A secondary metal site may also bridge two cluster sites rather than associate with the single cluster. Similarly, the clusters may exhibit variable loci for attachment to the secondary metal−ligand component. The relative dispositions of the linkage points on the surface of the cluster synthon are also variable and will influence the assembly of the building blocks. Consequently, the dynamic nature of the hydrothermal reaction domain and the structural versatility of the component substructures result in a diverse structural chemistry but also render absolute structural predictability problematic. The emerging structural systematics suggest that, as the structural database continues to evolve, the correlations of structure, reactivity, and properties will emerge more fully.

Acknowledgment. This work was supported by a grant from the National Science Foundation (CHE-0242153).

Supporting Information Available: Tables of atomic positional parameters, bond lengths, bond angles, anisotropic thermal parameters, and calculated hydrogen bond positions for **1**−**10** in CIF format. This material is available free of charge via the Internet at http://pubs.acs.org.

IC049201K